lubricants

MDPI

Review

Unveiling the Effect of Particle Incorporation in PEO Coatings on the Corrosion and Wear Performance of Magnesium Implants

Yasir Q. Almajidi [1], Eyhab Ali [2], Madiha Fouad Jameel [3], Luma Hussain Saleh [4], Saurabh Aggarwal [5], Sajad Ali Zearah [6], Abbas Firras Alamula [7], Ali Alsaalamy [8], Fariborz Sharifianjazi [9] and Masoud Soroush Bathaei [10,*,†]

1 Department of Pharmacy (Pharmaceutics), Baghdad College of Medical Sciences, Baghdad, Iraq
2 Department of Pharmacy, Al-Zahraa University for Women, Karbala, Iraq
3 Department of Dentistry, Al-Rafidain University College, Baghdad, Iraq
4 Department of Anesthesia Techniques, Al-Noor University College, Nineveh, Iraq
5 Department of Mechanical Engineering, Uttaranchal Institute of Technology, Uttaranchal University, Dehradun, India
6 Scientific Research Center, Al-Ayen University, Thi-Qar, Iraq
7 College of Technical Engineering, The Islamic University, Najaf, Iraq
8 College of Technical Engineering, Imam Ja'afar Al-Sadiq University, Al-Muthanna, Iraq
9 Department of Natural Sciences, School of Science and Technology, The University of Georgia, Tbilisi, Georgia
10 Department of Materials Engineering, Science and Research Branch, Islamic Azad University, Tehran, Iran
* Correspondence: ms.bathaei@gmail.com
† Current address: Department of Mining and Materials Engineering, McGill University, Montreal, QC H3A 0E8, Canada.

Abstract: Magnesium has been a focal point of significant exploration in the biomedical engineering domain for many years due to its exceptional attributes, encompassing impressive specific strength, low density, excellent damping abilities, biodegradability, and the sought-after quality of biocompatibility. The primary drawback associated with magnesium-based implants is their susceptibility to corrosion and wear in physiological environments, which represents a significant limitation. Research findings have established that plasma electrolytic oxidation (PEO) induces substantial modifications in the surface characteristics and corrosion behavior of magnesium and its alloy counterparts. By subjecting the surface to high voltages, a porous ceramic coating is formed, resulting in not only altered surface properties and corrosion resistance, but also enhanced wear resistance. However, a drawback of the PEO process is that excessive pore formation and porosity within the shell could potentially undermine the coating's corrosion and wear resistances. Altering the electrolyte conditions by introducing micro- and nano-particles can serve as a valuable approach to decrease coating porosity and enhance their ultimate characteristics. This paper evaluates the particle adhesion, composition, corrosion, and wear performances of particle-incorporated coatings applied to magnesium alloys through the PEO method.

Keywords: magnesium implants; plasma electrolytic oxidation; particles incorporation; composite coatings; corrosion behavior; wear resistance

Citation: Almajidi, Y.Q.; Ali, E.; Jameel, M.F.; Saleh, L.H.; Aggarwal, S.; Zearah, S.A.; Alamula, A.F.; Alsaalamy, A.; Sharifianjazi, F.; Bathaei, M.S. Unveiling the Effect of Particle Incorporation in PEO Coatings on the Corrosion and Wear Performance of Magnesium Implants. *Lubricants* **2023**, *11*, 519. https://doi.org/10.3390/lubricants11120519

Received: 13 September 2023
Revised: 12 October 2023
Accepted: 28 November 2023
Published: 8 December 2023

1. Introduction

In various engineering applications, magnesium and its alloys find extensive use, extending beyond the transportation industry where weight reduction is crucial [1]. They are also utilized in the production of biodegradable orthopedic implants [2]. The distinctive properties of magnesium and its alloys, including a suitable Young's modulus, high specific strength, biocompatibility, natural degradation, and osteopromotion, position them as revolutionary biometals [3,4]. With a Young's modulus close to that of bone, around 45 GPa,

and a density of approximately 1.74 g/cm^3, magnesium and its alloys offer promising applications in bone repair and implant technology [5–7].

In contrast, the density of alloys is determined by the elements included, similar to the density of human bones [8]. The good mechanical properties and low density of magnesium alloys make them an excellent choice for biodegradable implants [9]. With degradable implants, patients do not have to undergo a second surgery, which is cost-effective and beneficial for them [10]. The slow load transfer from the implant to the damaged area allows the damaged bone or tissue to heal faster [11]. A biodegradable implant must, however, be controlled so that degradation does not occur faster or slower than the time necessary for healing to ultimately happen [12,13]. As we have already discussed, magnesium-based implants offer all the advantages listed above, making them a suitable material for use as a biodegradable implant [14]. As a result of the efforts of researchers, magnesium alloys have been modified to have improved corrosion and mechanical properties, making them suitable for bone repair [15]. As part of the bone fixation system, there may be several components, including a bone plate, bone pin, bone screw, and so forth, each of which plays a vital role during the healing process [16,17]. Magnesium stents are medical devices made from magnesium alloys and they are used for various vascular applications, particularly in cardiology [18]. These stents are designed to be temporarily implanted in blood vessels to help support and maintain their structural integrity. Over time, magnesium stents gradually degrade and dissolve within the body, eliminating the need for a permanent implant [19]. Figure 1 illustrates a few of the most common magnesium biomedical devices currently used in surgery [20].

Figure 1. Biomedical applications of magnesium and its alloys: (**a**) cardiovascular stents and (**b**) orthopedic implants. Figure adapted with permission from [20].

Despite magnesium's excellent biocompatibility, a significant obstacle to its use in biodegradable implants in biomedical applications is its rapid in vivo corrosion [21]. The accumulation of hydrogen gas and the substantial increase in local pH may result in blocking of the bloodstream, necrosis of tissues, or even death due to the release of hydrogen gas [22]. To develop magnesium-based implants, it is crucial to control the rate of corrosion and degradation in the human body [23].

Despite their advantages, the comparatively lower wear resistance of magnesium alloys requires careful scrutiny to ensure the durability and efficacy of implants. Wear resistance is crucial for minimizing complications related to implant wear, such as particle generation and inflammation. This is especially vital in orthopedic applications, particularly

in load-bearing joints, where the wear resistance of magnesium implants becomes essential to prevent premature failure and improve patient outcomes [24].

Applying surface coatings and alloying is thought to be very effective at preventing the corrosion and wear rate and for achieving a reasonable service life [25,26]. The low solubility of some alloying elements in the magnesium matrix, although a feasible option to control the degradation rate of magnesium, remains a problem. The surface treatment of magnesium implants has been subjected to various techniques [27–29]. Plasma electrolytic oxidation (PEO, also known as micro-arc oxidation (MAO)) coats lightweight metals and alloys with ceramic-like coatings [30,31]. PEO coatings have two layers in their morphology: an amorphous outer film exhibiting pores and coarse morphology and a crystalline inner film showing delicate pores [32,33]. Amorphous elements within the inner film may crystallize due to oxygen production. As a result, it is unlikely that PEO coatings can prevent the formation of high porosity, especially for magnesium alloys, and the behavior of layers is also constrained due to the limited effect of the electrical parameters on the coating composition [34]. Modifying the composition of the electrolyte is another method for optimizing the design and microstructure of coatings to improve their properties [35]. Recently, advances have been made in this field that aim to add particles to the solution, thereby achieving in situ incorporation or sealing porous PEO coatings and providing new features to the coatings [36]. The PEO processes are affected by the addition of particles to the solution. As a result, it may alter the morphology and properties of the layer due to changes in the solution, such as pH, conductivity, and viscosity [37,38]. It is noted as an unmoving incorporation when particles are combined without a new phase being formed or without any reaction taking place. In other words, the particle shapes and sizes have not changed significantly. Another possibility is reactivity or a slight reactivity of the incorporation [39,40]. Because of high-energy discharges in the PEO process and reactions with other matrix and electrolyte elements, this condition may result in the melting of particles [41]. Numerous parameters are involved in this complex process, including substrates, electrolyte compositions, particle concentrations, Zeta potentials, melting points, and energy supply from discharges [42]. This review paper provides an overview and critical analysis of the effects of dissimilar particles on the PEO procedure, composition of coatings, and corrosion and wear performances of magnesium-based implants.

2. Corrosion and Wear Behavior of Magnesium-Based Implants

Magnesium alloys face challenges of low corrosion resistance and rapid degradation, primarily due to physiological solutions containing chloride ions that induce corrosion. Although a magnesium hydroxide film forms as a protective barrier, it is insufficient, leading to substrate exposure and increased corrosion risk, jeopardizing the mechanical integrity of implants and potentially causing premature failure [43–46]. Rapid degradation can impede correct integration of magnesium implants with bone, as magnesium reacts with water in body fluids, releasing hydrogen gas and hydroxide anions [44,45]. Magnesium ions, released during oxidation, can migrate into cells and tissues, influencing cellular structures and promoting viability, growth, and recovery [46]. The corrosion process, generating hydrogen gas, hydroxide ions, free radicals, and altering pH, can impact immune cells, influencing inflammation and wound healing [47]. Figure 2 illustrates potential reactions on magnesium surfaces [48]. These corrosion-related challenges underscore the need for comprehensive examination to enhance the performance and longevity of magnesium implants in biomedical applications [48].

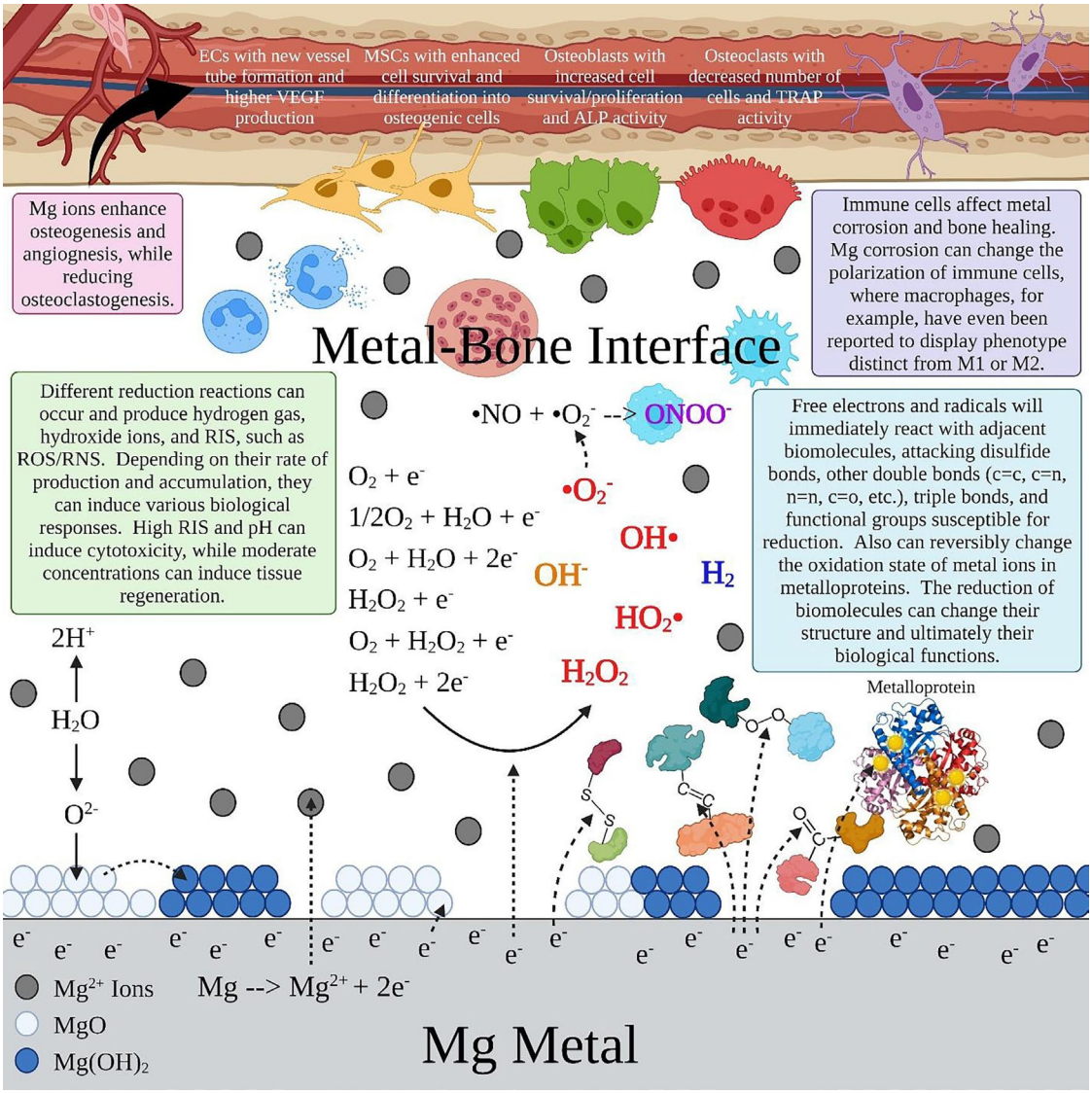

Figure 2. Corrosion behavior of magnesium metal at the metal–bone interface. Figure adapted with permission from [48].

The wear resistance of magnesium implants directly correlates with their longevity and durability within the human body [49]. Implants subjected to repetitive mechanical stresses, as seen in joints during daily activities, must withstand wear to maintain their structural integrity over an extended period. Enhancing wear resistance ensures a prolonged service life for magnesium implants, reducing the need for early replacements and associated surgical interventions. Their susceptibility to abrasive wear, corrosion-induced wear, and frictional heat generation necessitate innovative solutions [50]. Limited hardness compared with traditional materials contributes to accelerated material loss. Surface deterioration over time and complex loading conditions in the body further accentuate wear concerns. Addressing these weaknesses through advanced materials science, including coatings and surface modifications, is crucial for optimizing the wear resistance of magnesium implants. Overcoming these challenges ensures the longevity, durability, and reliability required for successful orthopedic interventions, making magnesium alloys a viable choice in the dynamic biomechanical environment of the human body [51].

3. PEO Process

As a result of plasma chemical, electrochemical, and thermal chemical reactions, the production mechanism for oxide coatings using PEO is complex [52]. The anodization of a magnesium substrate during the PEO process involves a series of electrochemical reactions. Here are the primary electrochemical reactions that occur during the anodization of magnesium [53]:

At the anode (Oxidation):

$$Mg \rightarrow Mg^{2+} + 2e^{-} \qquad \text{Oxidation of magnesium} \qquad (1)$$

This reaction involves the conversion of magnesium on the substrate's surface into magnesium ions (Mg^{2+}) by releasing two electrons. This fundamental reaction leads to the formation of the magnesium oxide (MgO) layer on the surface.

At the cathode (reduction):

$$O_2 + 4e^{-} + 2H_2O \rightarrow 4OH^{-} \qquad \text{Reduction of oxygen } (O_2) \qquad (2)$$

Oxygen gas (O_2) can be reduced to form hydroxide ions (OH^{-}) by gaining four electrons at the cathode. This reaction typically occurs in the surrounding electrolyte and contributes to the production of hydroxide ions.

$$2H_2O + 2e^{-} \rightarrow H_2 + 2OH^{-} \qquad \text{Formation of Hydrogen Gas } (H_2) \qquad (3)$$

In addition to the reduction in oxygen, another common cathodic reaction is the formation of hydrogen gas (H_2) through the reduction in water (H_2O) with the gain of two electrons. These reactions collectively drive the anodization process in PEO [54]. At the anode, magnesium undergoes oxidation to create magnesium ions (Mg^{2+}), which then react with oxygen ions and hydroxide ions to form the primary component of the coating, magnesium oxide (MgO). At the cathode, the reduction in oxygen and the formation of hydrogen gas help to maintain the charge balance in the system [55,56].

It is important to note that the PEO process may involve more complex reactions and intermediates, such as the production of the oxide coating, the breakdown of the dielectric layer, the dissolution of preexisting layers, and gas anodic evolution [57,58]. It depends on the magnesium alloy composition, the nature of the solution, and the concentrations of the constituents used, along with the current density of the reaction, which determines the dominance of any of these reactions [59]. Concerning the breakdown voltage time, the voltage appears to increase rapidly and linearly. Tiny bubbles of oxygen can be observed on the surface of specimens, and a thin oxide layer indicates the traditional anodizing process [60]. An ignition discharge occurs when the applied voltage exceeds a critical value, which causes the dielectric to break down [61]. During this stage, the current is concentrated within zones of breakdown, resulting in locally thickened oxide coatings. Unlike other areas with less resistance, the new layer is less resistant to current flow, reducing its resistance to leakage [62]. There is an accidental spreading and rapid movement of several tiny white sparks over the entire anode surface in conjunction with a shrill sound [63,64].

Oxide film production is continuous and breaks down, causing fluctuations in the potential. It is possible to produce ceramic oxide coating directly by gasifying the electrolyte and the valve metal [65]. During the growth of the oxide layer, a weak point results in the coating breaking down. The increment of the processing time results in more extensive discharge sparks, changing colors from white to red or orange [66,67]. A micro-arc becomes a strong arc in this zone. When gas is released and intense sparks occur, the film experiences thermal cracking and the formation of large pores. As the voltage declines rapidly, the gas bubbles and sparks disappear, indicating that the PEO process is ending [68].

A two-layer structure has been observed for magnesium, and a thin barrier film characterizes its alloys applied directly to the substrate and a porous outer layer that can be used to apply paints, polymer coatings, or other adhesives to the surface [69]. Despite

this, several limitations are associated with the PEO technique, including a limited range of compositions, high porosity, and high energy consumption. In general, the properties of PEO coatings are determined mainly by the design and microstructure, controlled by factors such as the method, solution, and substrate used to create them [70]. Optimizing the electrolyte composition is an effective strategy to enhance the properties of PEO coatings. Changing the design of the solution is an effective method to improve the microstructure and behavior of PEO oxide films. For most research studies, particle addition is just in the form of powders or sols added to solutions [71]. Sols are more malleable and present more substitutions than particles because of their substrate, for example, particle reinforcement within metal matrix composites. Additionally, in situ particle formation may occur during the PEO process if the solubility of a specific compound is exceeded. Particle-bearing solutions are thus considered with these methods. In this case, ensuring that the particles are dispersed evenly in the aqueous solution is challenging [72]. It seems that the predominant mechanism for incorporating fine particles into the coating entails their penetration into surface pores or indentations as a component of the PEO discharge cycle. This cycle occurs after the expansion and collapse of the plasma "bubble", leading to the replenishment of electrolytes [73]. Figure 3 presents a schematic depiction of a single electrolyte cycle with fine suspended particles in relation to the surface area of the discharge pores [74].

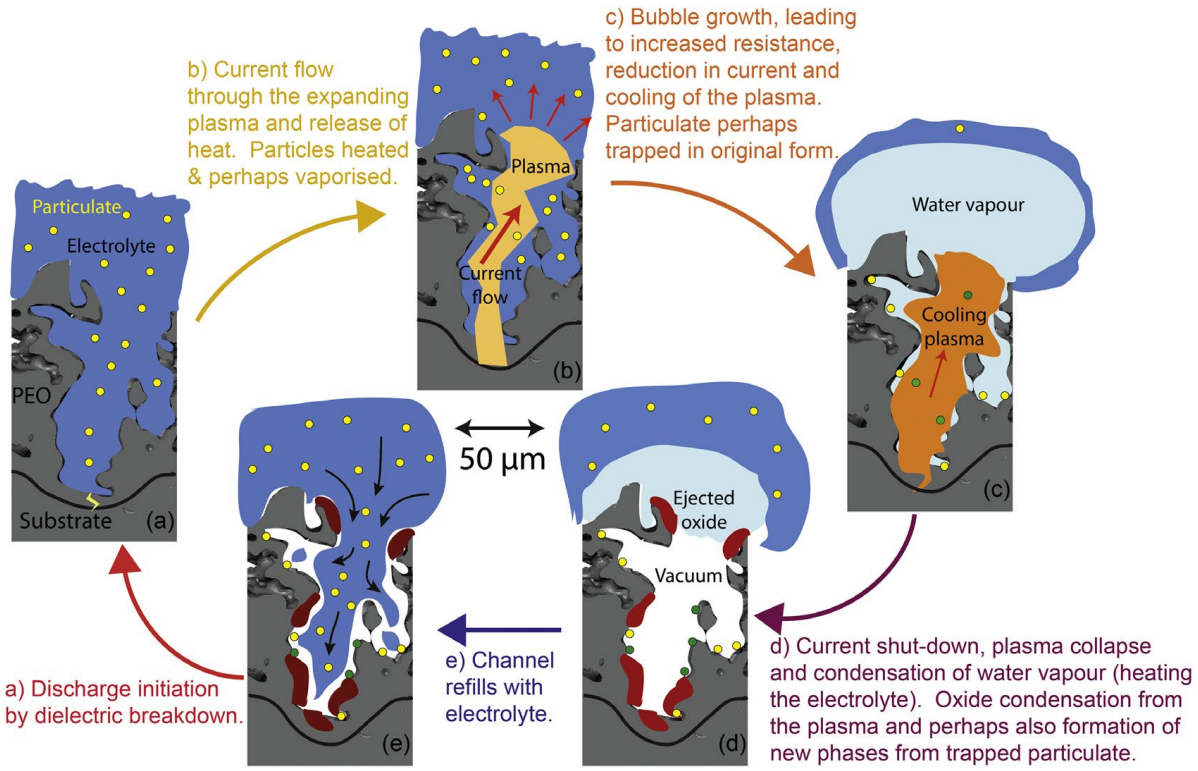

Figure 3. Schematic portrayal of an individual PEO discharge sequence featuring an electrolyte containing suspended particles. Figure adapted with permission from [74].

4. The Effect of Incorporated Particles on PEO Process

The incorporation of solid particles into the electrolyte during the PEO process can exert distinct effects on various electrical parameters. These effects are contingent upon factors such as the particles' type, concentration, and conductivity, as well as overall process conditions [75]. The presence of particles may necessitate voltage and current adjustments to achieve specific coating properties and ensure consistent process outcomes. Moreover, particle concentration can influence the overall electrolyte conductivity, which, in turn, affects the electrical current conduction in the system [76]. The spark discharge characteris-

tics may be altered by particle presence, potentially affecting the energy distribution within the PEO process [77].

Consequently, energy efficiency and consumption may be influenced, necessitating adaptations to maintain optimal efficiency. The system's electrical impedance and Zeta potential can also be impacted by particle incorporation, with implications for understanding the electrical behavior of the coated surface [78]. Additionally, particle presence can influence sparks' formation, distribution, and characteristics, leading to variations in the electrical behavior across the coating's surface. The system's electrical contact and charge transfer may exhibit differences due to solid particles, affecting resistance and charge transfer processes. These effects highlight the complexity of electrical parameters in PEO and underscore the importance of careful parameter control to attain the desired coating quality and performance [79].

Particles are often added to solutions as powders or sols in many studies. Compared with particles diminishing over the substrate, they have greater flexibility and provides a broader range of options [80]. Additionally, the formation of in situ particles may occur during PEO if the solubility of some compounds exceeds the extent of solubility in the electrolyte. In addition, these methods may also be identified as electrolytes that contain particles. A significant challenge in preparing PEO is achieving uniform particle dispersion in the electrolyte. In solid–liquid interfaces, the zeta potential is an essential factor that explains the charging behavior. The magnitude of the zeta potential measures electrostatic repulsion between adjacent particles in an electrolyte. A particle with a high value of Zeta potential is more stable, which allows it to avoid adhering to other particles and settling in PEO's electrolyte. Under a specific electrical field, having a high Zeta potential is advantageous as this enhances the movement rate of the particles [81,82].

Adding new ingredients to the electrolyte can affect the PEO process's electrical response. When particles are added to the PEO treatment bath, it has been demonstrated that the voltage ramp can be slowed down [83]. In the presence of Al_2O_3 particles, researchers observed a delay in the voltage ramp. Others have claimed that PEO processing has a decreased voltage if CeO_2 particles are added to the electrolyte. It should be noted, however, that other researchers have reported conflicting results regarding the voltage response and final voltage. A recent study indicates that PEO coatings can grow more rapidly and reach higher final voltages by adding Al_2O_3 nanoparticles [84].

Moreover, PEO processing is affected by the particle size. A reduction in the size of nanoparticles during PEO treatment can enable a more rapid transition of the voltage/current characteristics than a reduction in the size of the microparticles [85]. According to the study, particle addition has no noticeable impact on the processing of PEO. When ZrO_2 particles were added to the PEO treatment, their effect on the growth rate of the coating and voltage response was minimal. As the pH and conductivity of the electrolyte were not significantly altered after particle addition, this discrepancy was likely caused by the differences in power supplies and electrical parameters utilized during the PEO process [86]. PEO will respond more positively to particles added to the electrolyte in the form of alcosol, as opposed to the addition of particles in the form of sand. As a result, the electrolyte conductivity is decreased due to the primary solvent in alcosol, namely ethanol. Based on the study's results, it has been found that the breakdown potential, final voltage, and layer growth rate increased enormously with the concentration of sol in the electrolyte [87]. As a side note, it has also been found that such a sol can delay coating growth if added to the electrolyte. When alumina sol was added to the electrolyte, the breakdown and final voltage were significantly reduced [88].

In comparison with the addition of powders to the electrolyte, the effect of particle addition via the sol route appeared to have a more significant influence on the electrical response of the PEO process. PEO's electrical response is influenced by the electrolyte's composition, conductivity, and viscosity, which the organic additives affect [89]. The influence of PEO treatment varies greatly depending on the base electrolyte, substrate,

particle properties (types and sizes), and power source. Therefore, an accurate picture is not available [90].

5. Incorporation of Particles into the Electrolytes and Mechanisms of Particle Absorption

Numerous recent studies have examined how particles are absorbed and incorporated into PEO coatings. Because the pores on the coating surface are filled with particles following PEO treatment, we considered them pathways for particles to enter the coating [91]. In addition to the concentration of nanoparticles inside the pores, researchers have confirmed that nanoparticles accumulate in the vicinity and inside the pores at a higher rate than in the other zones [92]. A short-circuit path between the outer and inner layers was thought to transfer the particles to the interface between the two layers. Despite the appearance of "soft" sparking, limited inward mass transfer of particles has been observed for three-layered coatings on magnesium, up to 50% of the intermediate layer (Figure 4) [93]. Because of the reduced voltage under the "soft" sparking regime, particles were less likely to be absorbed. There has been a proposal for three significant steps, which led to the incorporation of nanoparticles into coatings: delivering particles to coating growth sites, trapping particles at those sites, and preserving embedded particles during the layering procedure [94]. According to other studies, the incorporation of particles into the coatings on magnesium alloy was primarily caused by electrophoretic deposition and mechanical mixing. PEO coatings on magnesium were also found to incorporate particles through electrophoretic deposition [95]. It has also been suggested that particle transfer from the electrolyte to the layer can be accomplished in two steps, uptake and incorporation. Positive particle uptake before the breakdown potential may be considered a deposition/adsorption process in the presence of anodic dissolution and strong re-deposition of conversion products [96].

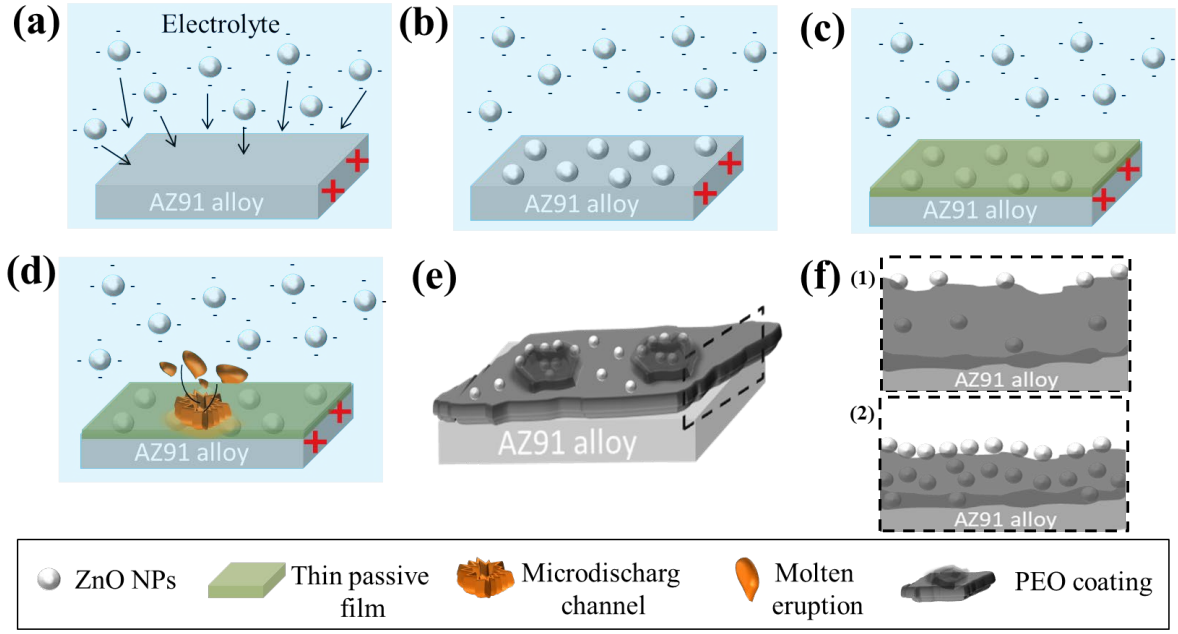

Figure 4. Coating growth mechanism: (**a**) Attraction of negatively charged ZnO NPs to the AZ91 magnesium alloy (anode) due to the electrophoretic effect. (**b**) Deposition of NPs onto the anode. (**c**) Formation of a thin passive film and entrapment of nanoparticles within this layer. (**d**) Microdischarging, localized melting, and eruption of molten oxide on the substrate. (**e**) Sintering and integration of NPs into the oxide coating. (**f**) Cross-sectional representations of PEO coatings fabricated with (**1**) a low concentration and (**2**) a high concentration of NPs in the electrolyte. Figure adapted with permission from [93].

It has been observed that particle size plays a significant role in the uptake process. Nanoparticles penetrate deeper into coatings than microparticles, based on the results of other studies [97]. Large particles, on the other hand, cannot penetrate through pores on the surface of the layer. Based on all of the studies related to this subject, it has been determined that particles can be incorporated in the PEO procedure by reactivity, relative reactivity, or infertility based on the electrolyte composition, the employed electrical factors, substrate, melting point, size, and chemical stability of the particle [98]. A mixture that results in no reaction or new phase formation is considered an inert incorporation. Incorporation can also be caused by reactive or relatively reactive responses arising from high-energy discharges that melt particles in the matrix and cause them to react with other components within the electrolyte [99]. A significant role would also seem to be played by the melting point of the particles in the incorporation process. For instance, SiC (2730 °C), CeO_2 (2400 °C), Si_3N_4 (1900 °C), and other high melting point particles were mostly inertly incorporated without considering their sizes. This procedure involved reactively incorporating particles with a kind of lower melting point [100].

Moreover, the particle size influences the mode of particle incorporation, coating properties, and, thus, the PEO process. For instance, ZrO_2 nanoparticles with a size of 150 to 300 nanometers have shown that, despite their high melting points, they react with magnesium to produce $Mg_2Zr_5O_{12}$. Even though the size of particles has been studied to determine their effects on PEO coatings, there are still many questions about their effectiveness [101]. Specifically, how particles with different melting points and sizes absorb and incorporate remains to be determined. There are also some unknowns and ambiguities regarding the intrinsic mechanism of adding particles to PEO coatings. Some researchers have claimed that the addition of ZrO_2 nanoparticles to the PEO coating causes short-circuiting in the outer film to move the nanoparticles to the interface between the outer and inner films [102]. Alternatively, other researchers found that the electrophoretic mobility of the particles within the magnesium oxide and the mechanical combining of molten magnesium oxides affected the incorporation of particles [103].

Moreover, the applied electrical factors play an essential role in specifying the form of incorporation of particles as the discharge lifetime and intensity directly correlate with the current density and voltage at all stages of the PEO process [104]. The PEO procedure dictates how the particles are absorbed and incorporated into the film based on particle properties (melting point and particle size) and electrical factors applied within the procedure [105]. A recent study revealed that the duties ratio, frequency, current densities, and voltages affect the particles' absorption within the PEO process. PEO coating can incorporate more particles at lower frequencies and higher duty ratios [106].

In the context of PEO of magnesium, introducing solid particles into the treated surface gives rise to intricate chemical and electrochemical reactions. These reactions occur at multiple interfaces involving the solid particles, the electrolyte, and the magnesium substrate [107]. In the electrolyte, water oxidation yields oxygen gas and hydrogen ions, while water reduction at cathodic sites generates hydroxide ions. When solid particles are immersed in the electrolyte, their dissolution can lead to the release of components into the surrounding solution. Concurrently, chemical reactions occur at the particle–electrolyte interface, forming hydroxides, oxides, or other compounds. The interaction between the solid particles and the magnesium substrate can entail species diffusion, like metal cations, from the substrate to the particle–substrate interface. This can lead to intermetallic compounds' development or surface chemistry's transformation [108].

Moreover, electrochemical reactions manifest at the magnesium substrate, with oxidation events leading to the formation of magnesium oxide. Reduction reactions at cathodic sites can involve hydrogen gas generation and oxygen reduction to hydroxide ions [109]. The amalgamation of these reactions contributes to the formation of the PEO coating and influences its chemical composition and microstructure. Furthermore, the responses can significantly impact the coated magnesium surface's corrosion resistance and other fundamental properties. It is essential to recognize that the precise reactions may vary depending

on various factors, such as the type of solid particles employed, the composition of the electrolyte, and the specific process conditions [110].

6. The Effect of Particle Incorporation on the Composition, Microstructure, and Morphology of PEO Coatings

As a result of the particles being introduced into the PEO process, it is clear that the microstructure and morphology of the coated surfaces loaded with particles differ from the particle-free surfaces [85]. The particles are part of the coating formation process. The application of PEO coatings on magnesium and its alloys has been modified using various oxide particles. Small oxide particles with low melting points and small sizes can generally be reactively incorporated much more readily than large oxide particles with high melting points [89]. The amorphous phase is present in the coatings due to the melting of small particles, which causes them to react with other ingredients and become amorphous. As a result, the coating composition obtained from a solution containing micro-sized particles did not differ substantially from that obtained from a solution without micro-sized particles, except for the presence of particles that were inertly incorporated into the composition [102]. PEO coatings are characterized by their microstructure, morphology, and composition, which are determined, in part, by the design of the PEO electrolyte [98].

Plasma electrolytic oxidation (PEO) coatings undergo significant changes in pore characteristics, compactness, and thickness with the introduction of oxide particles, influencing their microstructure and morphology. Incorporating oxide particles into electrolytes reduces the number and size of pores on the coating surface, exemplified by the notably reduced surface porosity observed with the addition of TiO_2 [83]. The efficacy of the sealing process is enhanced when a sol is introduced into the electrolyte, and oxide particles generally do not significantly alter the coating surface or increase porosity [76]. Coatings formed in particle-free electrolytes exhibit a more uniform and compact outer layer, while the impact of particle size on coating thickness lacks a clear trend [80]. Conflicting results exist regarding the effect of oxide particles on coating thickness, with some studies reporting no enhancement or even thinning, while others suggest increased thickness [105]. Changes in voltage/current evolution during PEO processing are associated with variations in the thickness of particle-containing coatings. ZrO_2 nanoparticles, introduced through electrophoretic interaction and mechanical mixing, are found to primarily occupy pores within the magnesium oxide layer, as depicted in Figure 5 [111].

Generally, non-oxide particles, such as metallic, organic, and inorganic particles, are inertly incorporated into PEO layers. There are also some cases in which part-reactive integration can be observed for calcium phosphate- and carbide-based particles when the discharge temperature and lifetime are sufficient for the particles to melt or decompose [112]. Different substrates, base electrolytes, and electrical parameters were used during the PEO process, which can explain the discrepancy. The incorporation of inert particles commonly reduces the porosity of PEO coatings. As a result of the incorporation of PTFE particles into the coating surface, the pores on the coating surface became finer and more homogeneous [113]. It has been reported that particle-containing coatings have a denser cross section as through-going pores and defects are virtually impossible to detect in these coatings. Thicker coatings were formed when SiC nanoparticles containing electrolytes were exposed to constant currents [114]. It depends on the current density applied to the coating to determine how thick it will become. Low current density results in a more significant value when compared with high current density. In contrast, the coatings obtained from particle-free electrolytes under a constant voltage mode were thinner than those produced in PTFE and Si_3N_4-containing electrolytes. The difference in incorporation modes and electrical parameters is likely to be the reason [115].

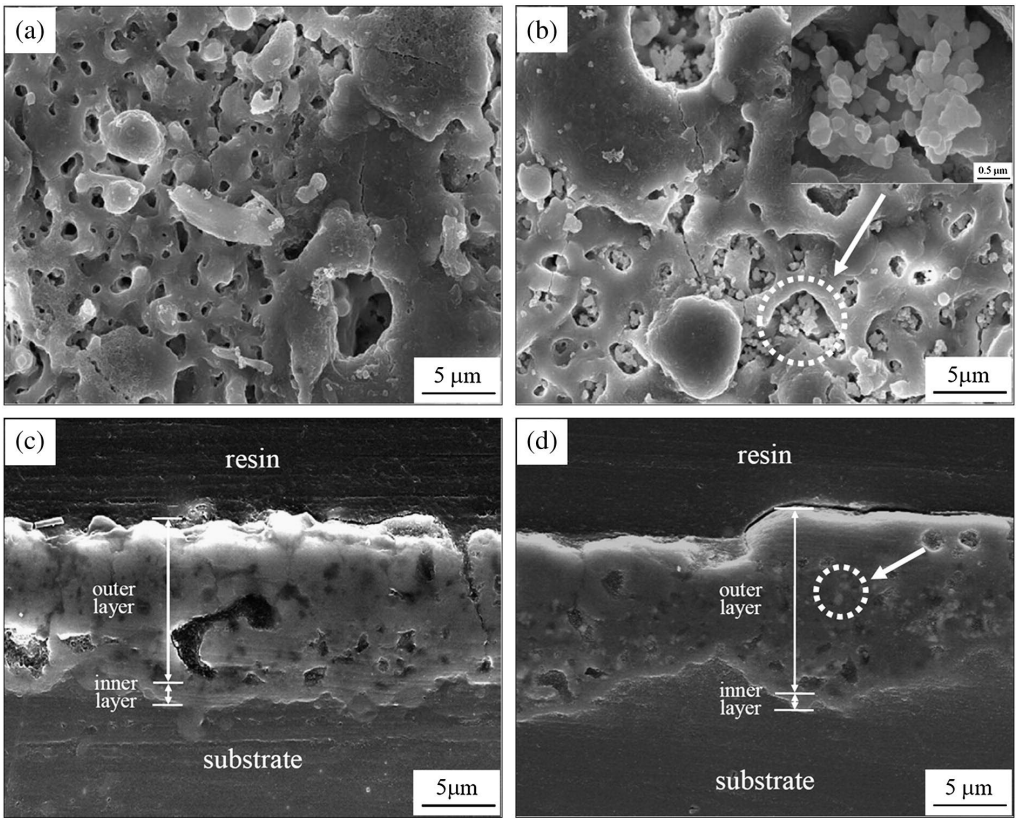

Figure 5. Surface morphologies of the oxide layer (**a**) without ZrO_2 and (**b**) with ZrO_2, and cross-sectional images of the oxide layer without (**c**) ZrO_2 and (**d**) with ZrO_2. The white arrows with dashed circles show the trapped particles inside pores. Figure adapted with permission from [111].

Regarding cross-sectional morphology, all coatings could be divided into three distinct zones: pore bands, outer films, and inner compact barrier films. PEO layers grow in opposite directions, with growth inwards toward the substrate and outwards toward the interface of the coating and solution, according to the reported growth mechanism. A constant ejection of molten material from the coating surface and its subsequent solidification can be attributed to the inward growth of the coating in thickness [98]. A band of pores was created because the growth dynamics in both directions were rarely identical, resulting in an unfilled zone within the coating. There was a significant difference in thickness between the outer film and the other two parts of the coating, with the outermost film containing more than half of the total coating thickness. Despite this, many observable defects were visible even when magnified relatively lowly [102]. Figure 6 depicts the (backscattered electron images) BSE cross-sections of the CeO_2-incorported coatings on the AM50 magnesium alloy, accompanied by X-ray elemental mapping of Si and Ce [116]. While the oxygen content remained consistent across all coatings, the presence of silicon diminished slightly in the coatings formed using CeO_2-containing electrolytes. As anticipated, cerium was only evident in coatings incorporating CeO_2, and its concentration increased with higher particle concentrations in the electrolyte. EDS point analyses conducted in areas with significant particle agglomeration revealed noteworthy shifts in the content of Ce and Si elements, with the Ce concentration rising to 10 atomic percent and the Si concentration decreasing to 7 atomic percent. The localized variations in coating composition were closely linked to the distinct characteristics of microdischarges and the preferred placement of particles within the coating pores [116].

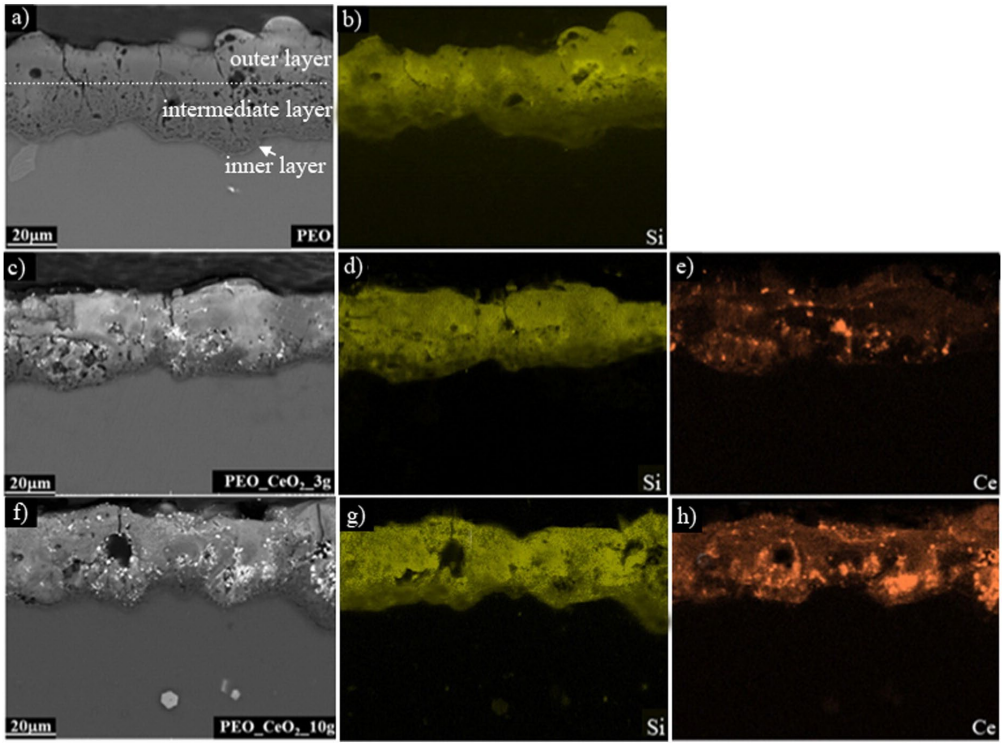

Figure 6. BSE images of the cross-sectional view, along with the corresponding X-ray elemental mappings for: (**a**,**b**) PEO and Si elements; (**c**–**e**) PEO_CeO_2_3 g, Si, and Ce elements; and (**f**–**h**) PEO_CeO_2_10 g, Si, and Ce elements. Figure adapted with permission from [116].

In the PEO of magnesium, an array of solid particles could be thoughtfully integrated into the electrolyte to yield distinctive enhancements. These particles, harnessed for specific purposes, encompassed diverse functionalities. Ceramic particles, exemplified by hydroxyapatite (HA) or tricalcium phosphate (TCP), are routinely introduced to foster bioactivity and augment osseointegration, emulating the mineral composition of bone tissue and facilitating the integration of bone onto the implant surface [117–120]. Metallic particles, like Ag or Cu, confer antibacterial properties to the coating. The inclusion of silver particles is renowned for its potent antimicrobial capabilities, effectively safeguarding against bacterial infections, especially in medical implants. Biocompatible nanoparticles, such as TiO_2, find their niche in the realm of PEO for magnesium, elevating the biocompatibility and corrosion resistance of the implant surface [121,122].

Furthermore, alloying elements, such as calcium or strontium, are strategically integrated, bolstering the coating's mechanical properties and corrosion resistance. Within the purview of PEO, there is also a burgeoning interest in infusing nanoparticles with anti-inflammatory agents or therapeutic drugs, creating coatings that can release these substances to mitigate inflammation and expedite the healing process at the implant site [123–125].

Developing hydrophilic PEO coatings on magnesium in biomedical implant applications relies on strategically incorporating specific particles. Examples of particles that enhance the hydrophilicity of PEO coatings include TiO_2 nanoparticles, renowned for their inherent hydrophilic properties, as well as SiO_2 and ZrO_2 nanoparticles, both known for their hydrophilic nature. The introduction of hydrophilic polymers like polyethylene glycol (PEG) can also be employed to increase the coating's affinity for water. Moreover, calcium phosphate nanoparticles, including HA, play a pivotal role in biomedical coatings, enhancing hydrophilicity and biocompatibility. These hydrophilic particles offer tailored solutions for optimizing the wettability of PEO coatings, ensuring their suitability for biomedical implants where interactions with physiological fluids and tissues necessitate hydrophilic surface properties [126].

Pioneering strides have also been made in tissue regeneration, with nanoparticles bearing growth factors and other bioactive molecules that serve as catalysts for tissue rejuvenation and heighten the implant's overall performance [127–130]. The selection of particles is inherently dictated by the PEO process's unique objectives and the magnesium implant's intended application. These particles operate in tandem with precise modifications to the coating's composition, structure, and properties, strategically tailored to fulfill the desired functional requirements. These can encompass vital aspects such as biocompatibility, corrosion resistance, antibacterial efficacy, or bioactivity, all converging to foster enhanced osseointegration and bolster the implant's clinical utility.

On the other hand, the inner film consists of just a couple of microns in thickness. However, some imperfections may be visible in the film and at the boundaries of the coating and substrate [85]. Hence, it is apparent that the formed coatings adhere firmly to the substrate and are corrosion resistant mainly due to the relatively compact inner layer of protection. In the last few years, it has been hypothesized that adding nanoparticles to the PEO reaction alters the evolution of voltage and current to change the coating thickness [69]. Based on the characteristics of the nanoparticles added, the thickness of the coating can either be enhanced or reduced. Oxide particles can alter or improve a layer's compactness and thickness. Comparing the coatings formed in particle-free electrolytes with those included in particle-rich electrolytes, the outer layer of the coatings became less compact and uniform. The influence of particles on coating thickness does not appear to be directly correlated [84]. Adding oxide particles to coatings did not enhance their thickness, as coating thickness typically remained the same or decreased. The layers, however, were reported to be a bit thicker when particles were present. During PEO processing, the voltage/current evolution is altered, which changes the thickness of the particle-containing coatings [131].

7. Corrosion Performance of PEO Coatings with Particle Incorporation

The corrosion of magnesium implants is governed by a series of electrochemical reactions at the implant's surface. At the anode, magnesium undergoes oxidation, releasing magnesium ions (Mg^{2+}) and liberating electrons (e^-), as represented by the following equation [132]:

$$Mg \rightarrow Mg^{2+} + 2e^- \quad (4)$$

Simultaneously, at the cathode, where oxygen (O_2) and water (H_2O) are present, reduction reactions occur, leading to the formation of hydroxide ions (OH^-). This reaction can be expressed as follows:

$$O_2 + 2H_2O + 4e^- \rightarrow 4OH^- \quad (5)$$

The overall corrosion of magnesium implants can be represented as the combination of these anodic and cathodic reactions, with the formation of magnesium hydroxide ($Mg(OH)_2$) as a common corrosion product. This corrosion process not only compromises the structural integrity of the implant, but also impacts its biocompatibility. Consequently, researchers are dedicated to developing protective coatings and corrosion-resistant alloys to mitigate the corrosion of magnesium implants and to enhance their long-term performance within the human body, particularly in the context of biodegradable magnesium-based medical implants [132].

As mentioned before, in a ceramic-like PEO structure, micropores and microcracks are inevitable for two reasons [133]. Aside from this, typically, electrical discharges, intense heat, and gas bubbles are formed on the surface of the PEO solution, leading to the formation of many microchannels, some of which do not solidify during the PEO process. It is also important to note that the Pilling–Bedworth (P-B) for magnesium oxide is considerably lower than that for metal, resulting in a loose layer of magnesium oxide forming on the metal's surface [134]. As a consequence of the quick solidification of molten oxide inside the solution within the cooling process, micro-cracks appear in the structure of oxide coating.

Electromagnetic microdischarges produce pores that allow corrosive ions to penetrate the coating, failing the protective layer [135]. The corrosion performance of a PEO coating in biological aggressive media and for long periods depends on several parameters, such as the composition, thickness, porosity, and defects within the coating. When pores and cracks are present in the oxide film, corrosion ions will be able to penetrate in irregular directions, resulting in a decrease in the protective properties of PEO coatings [136,137].

The corrosion behavior of PEO coatings on magnesium and its alloys has been improved using different particles, but controversy has also been raised regarding the results [138]. The increase in corrosion properties can be attributed primarily to the formation of new stable phases (reactive incorporation of particles) and incorporating inert particles into a magnesium oxide coating with a high chemical stability [139]. It has been investigated how the PEO coatings behaved under corrosion and how they performed in terms of corrosion resistance on magnesium and its alloys. Different tests, including open circuit potential (OCP), potentiodynamic polarization (PDP), and electrochemical impedance spectroscopy (EIS) have been conducted. As PDP has been used in most studies, the results of this study will focus on PDP tests. The corrosion potentials (E_{corr}) and corrosion current densities (i_{corr}) for PEO-coated samples with and without particles were extracted based on the PDP curves. The extracted data are listed in Table 1.

Table 1. The comparison of the PDP results of particle-incorporated PEO coatings on magnesium alloys.

Substrate	Incorporated Particle Type	Corrosive Media	Without Particles		With Particles		Ref.
			E_{corr} (mV)	i_{corr} ($\mu A.cm^{-2}$)	E_{corr} (mV)	i_{corr} ($\mu A.cm^{-2}$)	
Pure Mg	La_2O_3	SBF	−1770	33.6	−1590	0.68	[92]
AZ91	ZnO	SBF	−1742	6.17	−1386	0.063	[93]
AZ80	CNT	3.5 wt% NaCl	−1380	2.5	−1250	0.56	[103]
AZ91	ZrO_2	3.5 wt% NaCl	−1400	0.727	−1300	0.07	[140]
AZ91	CeO_2	3.5 wt% NaCl	-	-	−360	0.478	[141]
AZ31	CeO_2	3.5 wt% NaCl	−1540	8.6	−1450	0.04	[142]
AZ31	MoS_2	3.5 wt% NaCl	−100	2.96	−1300	0.83	[143]
AZ31	SiC	3.5 wt% NaCl	−1485	1.84	−1470	0.13	[144]
AZ31	WC	3.5 wt% NaCl	−1460	31.85	−1451	10.23	[145]
AZ31	GO	3.5 wt% NaCl	−1490	0.124	−1440	0.033	[146]
AZ31	HA	SBF	−1610	4.77	−1540	0.123	[147]
MA8	TiN	3 wt% NaCl	−1370	0.12	−1440	0.14	[148]
AM50	SiO_2	0.5 wt% NaCl	−1449	1.2	−1556	0.19	[149]
AM50	Clay	0.5 wt% NaCl	−1477	63	−1542	58	[150]
Mg-Li	Graphene	3.5 wt% NaCl	−1600	1.2	−1512	0.106	[151]
AZ31	HA/GO	SBF	−1598	122.1	−1472	36.43	[152]
ZK60	CeO_2/ZrO_2-HA	SBF	-	-	−1289	43.84	[153]
AZ31	ZnO	Hank	−1390	0.65	−1461	0.08	[154]
AZ31	Al_2O_3	3.5 wt% NaCl	−1561	18.89	−1509	0.65	[155]
Mg-Li	TiO_2	3.5 wt% NaCl	−1529	4.409	−1.495	1.725	[156]
AZ91	Graphite	0.5 wt% NaCl	−1700	2.0	−1720	0.6	[157]
AZ80	PTFE	0.5 wt% NaCl	−1520	0.878	−1510	0.161	[158]
AZ31	WO_3	3.5 wt% NaCl	−1820	0.077	−1670	0.021	[159]

E_{corr}: corrosion potential; i_{corr}: corrosion current density; SBF: stimulated body fluid; GO: graphene oxide; HA: hydroxyapatite; CNT: carbon nanotube; PTFE: polytetrafluoroethylene.

Corrosion occurrence thermodynamic tendency generally decreases as E_{corr} increases. i_{corr} indicates the corrosion rate of samples, and the corrosion resistance is primarily determined by this [138]. As the i_{corr} increases, corrosion resistance decreases [139]. Compared with uncoated substrates, PEO-coated samples showed a lower i_{corr} in PDP curves and data in Table 1. Accordingly, the PEO coatings offered higher corrosion resistance than the substrates that were not coated. It can also be seen that corrosion resistance was improved by adding particles to the composition of electrolytes. Upon deposition, the coating inhibited the transfer and penetration of ions from the surface to the substrate by protecting

them from electrochemical reactions. A layer of this coating also prevented the substrate from being demolished by electrochemical reactions. Adding particles to the coating enhanced the disorder in the electrochemical reactions by filling the PEO coating defects like porosities/cracks and inhibiting ion transfer from aggressive biological solutions [160].

Ma et al. showed that the addition of TiO_2 nanoparticles (2, 4, and 6 g/L) to PEO coatings on Mg-Li magnesium substrates had a significant effect on their properties [156]. The addition of TiO_2 nanoparticles in the solution at concentrations lower than 4 g/L produced more uniform and thicker coatings with smaller micropores than those that would have been formed in the solution without nanoparticles. It is important to note, however, that TiO_2 nanoparticles can generate thermal solid effects that can decrease the corrosion resistance of coatings as they form cracks, as was highlighted by the addition of 6 g/L of TiO_2 nanoparticles. As a result of Rehman et al.'s investigation, small particles of CeO_2 were observed to affect both the final microstructure of the coating within the solution and the corrosion behavior of the layer [141]. The coatings were formulated with CeO_2 particles that were positioned preferentially in the pores and cracks of the layers. As a result of this process, both the reactive and rising absorbance of CeO_2 were affected, as well as the CeO_2 under local melting, made possible by microdischarges. During the coating process, lower concentrations of CeO_2 lead to an incomplete blocking of pores and cracks. However, an increase in particle concentrations up to 10 g/L resulted in a more complex structure, with more unsealed pores and cracks. This study of the short-term corrosion performance of PEO-coated samples was conducted through an analysis of their microstructures; therefore, PEO-CeO_2-3 g/L displayed the highest overall resistance, and PEO-CeO_2-10 g/L showed the lowest resistance in comparison with PEO coatings without the addition of CeO_2. An experiment conducted by Seyfoori et al. investigated the influence of adding hydroxyapatite (HA) nanoparticles to the AZ31 magnesium alloy (5, 10, and 15 g/L) on the material's properties [147]. As the uncoated sample was produced while exposed to the atmosphere, a porous oxide film formed on it. According to Nyquist's diagram, the uncoated sample underwent inductive treatment, as the oxide film of the corrosion-resistant solution traversed the surfaces of the metals and attained the substrate when immersed in the corrosive electrolyte. Because of their low corrosion resistance, this produced an induction behavior. Based on the Nyquist diagram, the coatings formed at various HA concentrations exhibited a similar behavior [147]. The fact that there were two capacitive loops in the coating and an inductive treatment implies that three procedures were present [90]. An inductive procedure revealed the corrosion procedure at low frequencies, with the loop produced at high frequencies connected to the outer porous film. In addition, the loop at high frequencies exhibited the inner dense film at medium frequencies. Inductive analysis revealed that the specimens were subjected to pitting corrosion. It has been demonstrated that an increase in HA NPs from 5 to 15 g/L increased the Nyquist loop diameter, which indicates an increase in the corrosion performance of the coating. The same behavior was reported by Wen et al. with the addition of GO along with HA in the PEO electrolyte. The EIS study results are shown in Figure 7 [152]. The presence of three loops indicated the involvement of three distinct kinetic processes in corrosion. In the case of both the HA/GO coating and the PEO coating, the high-frequency loops (1–10 kHz) were associated with the outer porous region, while the medium-frequency loops (0.1–1 Hz) were attributed to the effects of the inner compact region formed during the PEO process. Within the frequency range of 0.001 to 0.1 Hz, there was a noticeable inductive response indicating the occurrence of pit corrosion in the samples [152].

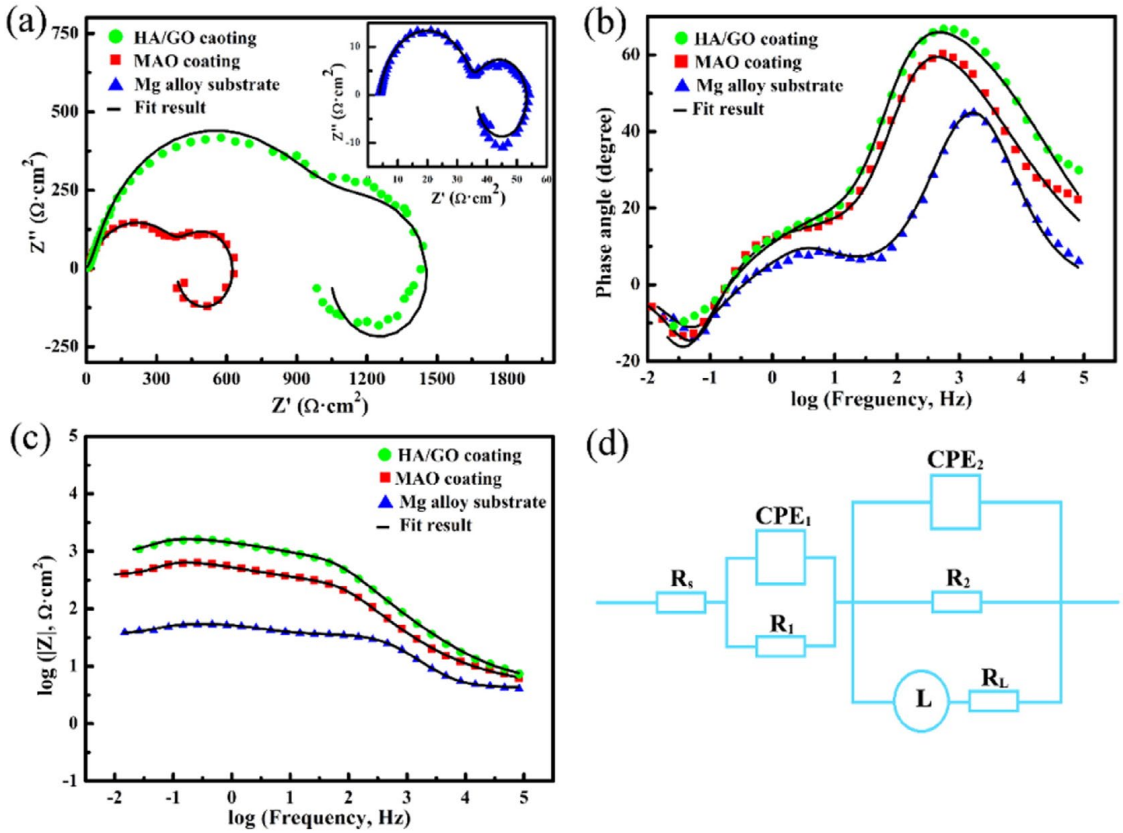

Figure 7. EIS measurements presented as a scatter plot and corresponding model fits displayed as solid plots for the magnesium alloy substrate, magnesium alloy with MAO coating, and magnesium alloy with HA/GO coating in a simulated body fluid (SBF) solution at 37 °C. (**a**) Nyquist plot, (**b**,**c**) Bode plots, and (**d**) equivalent circuit. Figure adapted with permission from [152].

It was proposed by Lu that particles with different melting points have different effects on the properties of PEO coatings. An alkaline-phosphate-based electrolyte was used to form PEO coatings on AM50, with and without including SiO_2, and clay [149,150]. Several studies have demonstrated that the reactive incorporation of clay particles results in the formation of a dense film, which in turn enhances the corrosion resistance of coatings. To determine the corrosion resistance of PEO coatings over the long term, electrochemical impedance spectroscopy (EIS) measurements were taken as the polarization test only provided limited information. A kinetic analysis of degradation was carried out using EIS to determine how the degradation process unfolded and how corrosion occurred. The Bode plots showed clear indications of a third relaxation procedure at high frequencies when examined in more detail. The response of the outer PEO film at high frequencies can be attributed to this time constant, while the response from the inner barrier film can be attributed to the medium frequency time constant. Furthermore, low-frequency relaxation can be associated with electrochemical activity at the interface between the metal and solution (capacitance of the double layer and resistance to charge transfer). According to Zhao et al., GO nanoparticles added to liquid (0, 1, 2, and 3 g/L, labeled as E0, E1, E2, and E3, respectively) harmed the corrosion properties [146]. The PDP study results are shown in Figure 8a. According to the study findings, the incorporation of GO into PEO coatings led to enhanced corrosion resistance. Coatings produced through the PEO process by adding 2 g/L GO exhibited a noteworthy uniformity, carbon content, and corrosion resistance enhancements. EIS results also revealed that compared with the 0 g/L specimen, the other three samples with GO within their PEO coating showed significantly larger capacitive loops, with the largest circle in the 2 g/L sample. A significant improvement in corrosion resistance was observed upon applying the PEO process, as evidenced by the

pronounced increase in impedance. According to electrochemical studies on the coatings, GO incorporation in the coating structures enhanced the corrosion performance of the PEO coatings. The PEO coating generated the highest uniformity, corrosion resistance, and carbon content due to the presence of 2 g/L GO during the PEO procedure. A concentration of GO in the solution resulted in an increased number of micropores on the coating surface and a decrease in the uniformity of the coating structures, thereby decreasing corrosion resistance. However, when the GO concentrations in the electrolyte exceeded 2 g/L, several factors such as an increased electrode surface area, heightened van der Waals forces, and stacking of GO tended to promote aggregation within the electrolyte, leading to coatings that did not exhibit the expected properties. Figure 8b illustrates that the PEO coating on sample E3 exhibited an expanded morphology characterized by a greater amplitude [146].

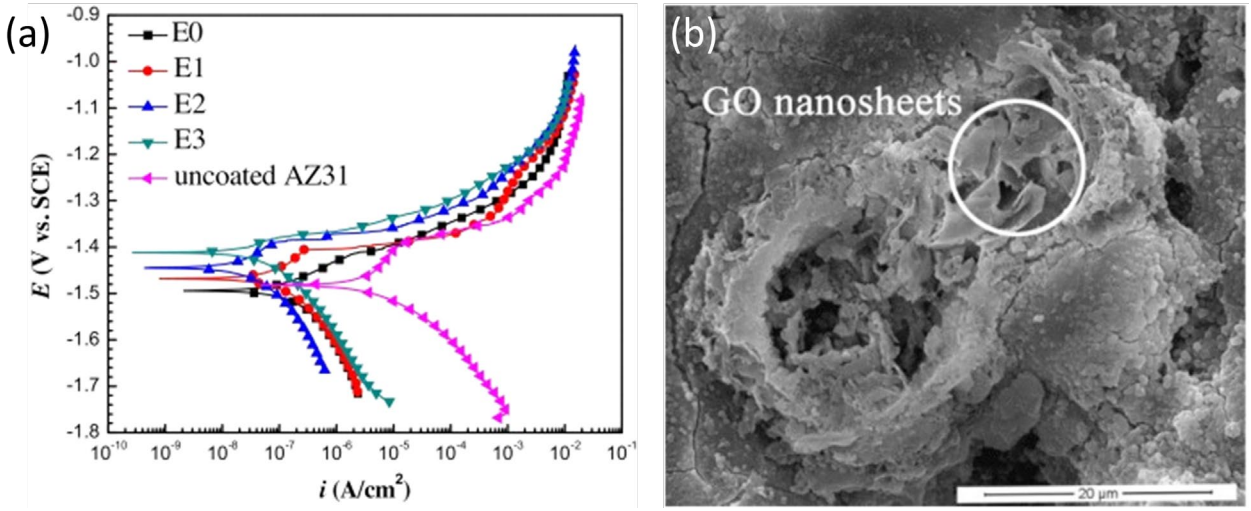

Figure 8. (**a**) PDP curves of the uncoated AZ31 sample and the GO-incorporated PEO coatings, and (**b**) trapped GO nanosheets in the PEO coatings porosity. Figure adapted with permission from [146].

During all of the electrochemical tests, it was found that the dense inner layers and inner layers of thick coatings offered better corrosion resistance than the porous outer layers. Adsorbent particles on the coating's surface encapsulated the external porous layers by filling cracks and micropores in the first step [140–160]. During the next step, particles moved to the interface of the internal/superficial layers through some of the pores and discharge channels of the external layer, and filled and sealed the internal layer defects and cracks. In this way, the particles decreased the porosity of the entire PEO coating and raised the resistance of the coating against penetration by corrosive media. Nano-particle-incorporated coatings versus corrosive ions is considered in terms of corrosion protection mechanisms. As several microcracks and micropores are present in coatings without nanoparticles, corrosive ions can penetrate these micropores and cause the substrate metal to rust. The nano-particles, however, have the additional capability of filling microcracks and microporosities in coatings during the PEO procedure, which can diminish the coatings' poor points concerning corrosion so that the diffusion of corrosive agents to the substrate metal is prevented. PEO coatings on magnesium and its alloys have been modified regarding the corrosion performance using distinct particles, but controversy has resulted from their application. In Figure 9, schematic representations of PEO coatings containing GO illustrate their ability to enhance corrosion resistance by effectively hindering the penetration of corrosive electrolytes into the magnesium surface [146].

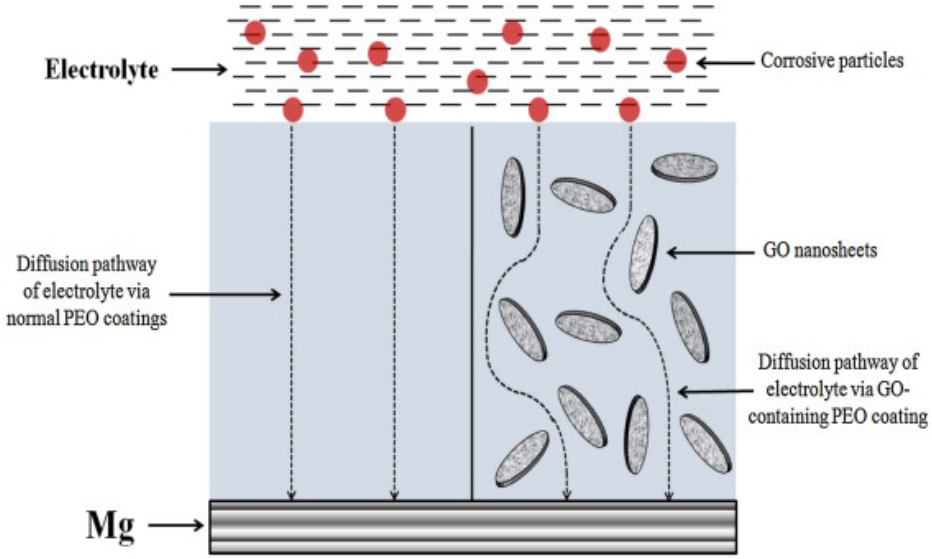

Figure 9. Schematic representation of the corrosion resistance of PEO coatings on magnesium substrates without and with GO particles. Figure adapted with permission from [146].

Finally, it can be mentioned that incorporating solid particles into PEO coatings on magnesium substantially enhances corrosion protection through diverse mechanisms. These particles instigate a multifaceted transformation in the coating's properties, shielding the underlying magnesium substrate from corrosive attack. Firstly, solid particles tend to increase coating density by infiltrating micropores and sealing voids, thereby minimizing the pathways for corrosive ions to penetrate the coating [161]. This results in a more uniform, impermeable structure that effectively guards against corrosion. Furthermore, particle incorporation exerts a profound influence on the microstructure of the PEO coating, leading to the refinement of grain boundaries and reduction in the size of defects, including cracks and pores. This finer microstructure not only strengthens the mechanical integrity of the coating, but also impedes the ingress of corrosive species, bolstering the protective qualities of the coating (Figure 10) [93].

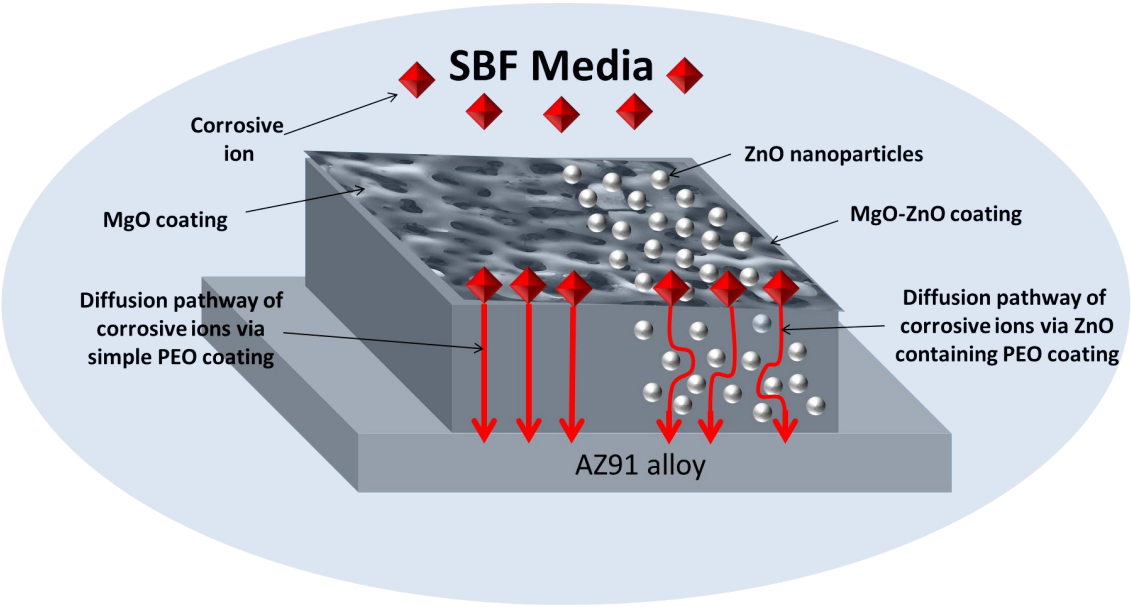

Figure 10. A schematic depiction of the corrosion protection offered by PEO coatings, both in their basic form and when incorporated with ZnO nanoparticles. Figure adapted with permission from [93].

Additionally, specific particles, particularly those rich in elements like aluminum or silicon, bring about chemical passivation of the magnesium substrate. This passivation process forms a protective barrier that actively inhibits the corrosion of the underlying magnesium, delivering long-term safeguarding against degradation [162].

Moreover, certain particles can react with the electrolyte and magnesium substrate, forming protective compounds, such as magnesium calcium phosphate. These compounds act as an additional barrier against corrosion, effectively blocking the intrusion of corrosive elements. Solid particles can also generate micro galvanic cells within the coating, leading to localized pH and potential changes, further inhibiting corrosion processes. Moreover, some particles function as pH buffers, stabilizing the local environment and thus offering protection against pH-induced corrosion [123]. The Zeta potential of particles plays a pivotal role in their incorporation into the coating, ensuring their adhesion and overall integrity, thereby minimizing the vulnerability of the layer to corrosion. Increased hardness, another outcome of particle addition, reinforces the PEO coating, making it more resistant to mechanical damage that could otherwise compromise corrosion protection. Finally, particle incorporation can influence the coating's surface energy and wettability, affecting how liquids interact with the surface. In specific cases, a hydrophobic surface is engineered, limiting the presence of moisture and thereby hindering corrosion processes [163]. It is paramount to recognize that the effectiveness and mechanisms vary depending on the particles' type, size, concentration, and chemical composition. Therefore, the selection of particles should align with the intended application and environmental conditions to optimize corrosion resistance. Electrochemically, these protective mechanisms can be linked to several reactions [132]. Passivation reactions involving the formation of oxide or compound layers on the magnesium surface play a central role, acting as barriers to corrosion. Redox reactions in the presence of certain particles can lead to the creation of protective compounds or modify the electrochemical behavior of the coating. Oxygen reduction reactions at the coating's surface may be affected by particle incorporation, influencing the corrosion rate. Solid particles can create micro galvanic cells, altering the local electrochemical behavior and inhibiting corrosion processes. Furthermore, certain particles may affect the local pH of the environment, thereby impacting corrosion rates through electrochemical methods. A comprehensive understanding of these mechanisms and their electrochemical underpinnings is indispensable for optimizing the design of PEO coatings, ensuring superior corrosion protection in diverse applications.

8. Wear Performance of PEO Coatings with Particle Incorporation

While magnesium alloys exhibit notable advantages as potential materials for orthopedic implants, it is essential to acknowledge and address their weaknesses, particularly in terms of wear resistance. Extending on this aspect provides a comprehensive understanding of the challenges associated with magnesium implants. Magnesium alloys are prone to abrasive wear, especially in scenarios involving contact with hard and abrasive surfaces [164]. The inherent softness of magnesium can result in accelerated material loss, leading to concerns about the long-term durability of implants. This susceptibility to abrasive wear emphasizes the need for strategies to mitigate surface damage and enhance wear resistance. Magnesium alloys are susceptible to corrosion in physiological environments. Corrosion products can act as abrasives, contributing to wear and material degradation. The combination of wear and corrosion, known as corrosive wear, poses a substantial challenge for magnesium implants. It necessitates the development of corrosion-resistant coatings or alloy modifications to mitigate the impact of corrosive wear on implant performance [165]. During wear processes, frictional forces generate heat, which can be a concern for magnesium implants. Elevated temperatures may contribute to thermal degradation and compromise the mechanical integrity of the implant. Managing frictional heat is crucial to prevent undesirable consequences such as surface cracking, increased wear rates, and potential inflammatory responses in the surrounding tissues. Magnesium alloys typically have lower hardness compared with traditional implant materials like titanium

and stainless steel [166]. This characteristic can lead to higher rates of material removal during wear, particularly in scenarios where implants experience contact with harder surfaces. Improving the hardness of magnesium alloys, either through alloying or surface treatments, is a key consideration for enhancing wear resistance. The surface properties of magnesium implants may deteriorate over time due to wear, potentially impacting their biocompatibility and mechanical stability. Surface modifications, coatings, and treatments must be designed to withstand the dynamic and challenging conditions within the human body, ensuring that the wear resistance of magnesium implants is maintained over the course of their intended service life [167]. Magnesium implants, especially those used in load-bearing joints, are subjected to complex loading conditions in the human body. Variability in loading patterns can contribute to uneven wear distribution, emphasizing the need for comprehensive testing and analysis to understand and address potential weak points in implant design, material selection, and wear-resistant strategies [168].

PEO coatings have gained prominence as a transformative technology for enhancing the wear resistance of magnesium implants. PEO coatings significantly augment the wear resistance of magnesium implants [169]. As mentioned earlier, by subjecting the magnesium surface to controlled plasma discharges, a ceramic oxide layer is formed, imparting superior hardness and wear resistance. Moreover, PEO-coated magnesium implants demonstrate remarkable resilience against abrasive wear [170]. The hardened ceramic layer serves as a robust barrier, minimizing direct contact between the magnesium substrate and abrasive surfaces. This property effectively mitigates material loss and extends the longevity of the implant. Importantly, the microstructure of PEO coatings contributes to effective temperature control during wear processes [171]. This is vital for preventing thermal degradation, maintaining the mechanical integrity of magnesium implants, and ensuring reliable performance under dynamic loading conditions. Furthermore, PEO enables tailoring of the surface characteristics, including the coating thickness, composition, and porosity. This versatility allows for customization based on specific wear requirements, optimizing PEO-coated magnesium implants for diverse orthopedic applications [172].

Incorporating particles into PEO electrolytes leads to composite coatings with enhanced wear resistance for magnesium implants. The introduction of particles, such as ceramics or nanoparticles, fortifies the coating matrix, providing additional hardness and reducing susceptibility to abrasive wear. Furthermore, particle addition allows for the customization of coating composition, enabling the creation of hybrid structures with unique properties. This tailoring process enhances the adaptability of PEO coatings to specific wear requirements, optimizing their performance for diverse orthopedic applications [173]. The incorporation of particles into PEO coatings influences the frictional characteristics during wear. Depending on the nature of the added particles, the coefficient of friction may be modified, contributing to improved tribological properties and better wear performance of the magnesium implants in dynamic conditions. It has also been reported that achieving an optimized dispersion of particles within the PEO coating is crucial for uniform properties across the surface. Proper dispersion ensures that the enhanced wear resistance and other desired characteristics are consistently distributed, promoting the reliability of the composite coating [174]. The choice of particles for addition to PEO electrolytes introduces versatility. Different particle types, sizes, and compositions can be selected to impart specific properties, such as increased hardness, improved lubricity, or tailored biocompatibility, contributing to a multifaceted approach to optimizing wear behavior [175]. Table 2 summarizes the wear test results data for PEO coatings on magnesium alloys, comparing cases with and without incorporated particles.

Table 2. The data of the wear test results for PEO coatings with and without particles on magnesium alloys.

Substrate	Incorporated Particle Type	Wear Rate of PEO Coatings without Particles	Wear Rate of PEO Coatings with Particles	Reduction of Wear Rate	Ref.
AZ31B	Al_2O_3	0.45×10^{-6} ($g \cdot Nm^{-1}$)	0.15×10^{-6} ($g \cdot Nm^{-1}$)	66.67%	[176]
AZ31		3.09×10^{-4} ($mg \cdot Nm^{-1}$)	1.55×10^{-4} ($mg \cdot Nm^{-1}$)	49.84%	[155]
AZ31		4.375×10^{-5} ($mm^3 \cdot Nm^{-1}$)	2.5×10^{-5} ($mm^3 \cdot Nm^{-1}$)	42.86%	[177]
AZ31B		8.3×10^{-3} ($mg \cdot Nm^{-1}$)	1.0×10^{-3} ($mg \cdot Nm^{-1}$)	87.95%	[178]
MA8	ZrO_2	4.1×10^{-5} ($mm^3 \cdot Nm^{-1}$)	2.9×10^{-5} ($mm^3 \cdot Nm^{-1}$)	29.27%	[179]
AZ31		4.1×10^{-5} ($mm^3 \cdot Nm^{-1}$)	2.9×10^{-5} ($mm^3 \cdot Nm^{-1}$)	29.27%	[180]
MA8	ZrO_2/SiO_2	4.3×10^{-5} ($mm^3 \cdot Nm^{-1}$)	3.2×10^{-5} ($mm^3 \cdot Nm^{-1}$)	25.58%	[181]
AM50	CeO_2	1.90×10^{-4} ($mm^3 \cdot Nm^{-1}$)	6.15×10^{-5} ($mm^3 \cdot Nm^{-1}$)	67.63%	[182]
AM50	SiO_2	3.7×10^{-3} ($mm^3 \cdot Nm^{-1}$)	7.3×10^{-4} ($mm^3 \cdot Nm^{-1}$)	80.27%	[149]
MA8		4.1×10^{-5} ($mm^3 \cdot Nm^{-1}$)	3.5×10^{-5} ($mm^3 \cdot Nm^{-1}$)	14.63%	[179]
AZ31	Ta_2O_5	1.1 ($\mu m^3 \cdot Nm^{-1}$)	0.1 ($\mu m^3 \cdot Nm^{-1}$)	90.91%	[183]
AZ31	SiC	3.8×10^{-4} ($mm^3 \cdot Nm^{-1}$)	3.3×10^{-4} ($mm^3 \cdot Nm^{-1}$)	13.16%	[184]
AZ31		14.57×10^{-4} ($mg \cdot Nm^{-1}$)	8.68×10^{-4} ($mg \cdot Nm^{-1}$)	40.43%	[144]
AZ31B		24×10^{-4} ($mg \cdot mN^{-1}$)	13×10^{-4} ($mg \cdot mN^{-1}$)	45.83%	[185]
AZ31B		5×10^{-3} ($mg \cdot m^{-1}$)	4×10^{-4} ($mg \cdot m^{-1}$)	92%	[186]
AZ91D		2.67×10^{-2} ($mg \cdot min^{-1}$)	1.33×10^{-2} ($mg \cdot min^{-1}$)	50.19%	[187]
AZ31		22.47×10^{-4} ($mg \cdot Nm^{-1}$)	9.49×10^{-4} ($mg \cdot Nm^{-1}$)	57.77%	[188]
AZ31B		28.65×10^{-4} ($mg \cdot Nm^{-1}$)	6.67×10^{-4} ($mg \cdot Nm^{-1}$)	76.72%	[189]
AZ31B	WC	15.20×10^{3} ($mg \cdot m^{-1}$)	5×10^{3} ($mg \cdot m^{-1}$)	67.11%	[190]
AZ31B		24.58×10^{-4} ($mg \cdot Nm^{-1}$)	11.86×10^{-4} ($mg \cdot Nm^{-1}$)	51.75%	[191]
MA8	TiN	1.1×10^{-5} ($mm^3 \cdot Nm^{-1}$)	5.0×10^{-6} ($mm^3 \cdot Nm^{-1}$)	54.55%	[192]
MA8		4.3×10^{-5} ($mm^3 \cdot Nm^{-1}$)	1.9×10^{-6} ($mm^3 \cdot Nm^{-1}$)	95.5%	[193]
MA8		4.3×10^{-5} ($mm^3 \cdot Nm^{-1}$)	1.9×10^{-5} ($mm^3 \cdot Nm^{-1}$)	55.81%	[194]
Mg–Li	WS_2	9.27×10^{-5} ($mm^3 \cdot Nm^{-1}$)	4.37×10^{-5} ($mm^3 \cdot Nm^{-1}$)	52.86%	[195]
AZ31	MoS_2	0.91×10^{-6} ($mm^3 \cdot Nm^{-1}$)	4.76×10^{-4} ($mm^3 \cdot Nm^{-1}$)	99.8%	[195]
Mg–Li	Graphite	9.27×10^{-5} ($mm^3 \cdot Nm^{-1}$)	4.80×10^{-5} ($mm^3 \cdot Nm^{-1}$)	48.22%	[194]
AZ31	Graphene	16×10^{3} ($mg \cdot m^{-1}$)	4×10^{3} ($mg \cdot m^{-1}$)	75%	[196]
AZ31	GO	5.62×10^{-4} ($mm^3 \cdot Nm^{-1}$)	1.34×10^{-4} ($mm^3 \cdot Nm^{-1}$)	76.16%	[197]

Oxide particles contribute significantly to wear resistance. These particles introduce heightened hardness, acting as formidable barriers against abrasive wear. Additionally, their incorporation fosters the development of a dense, stable oxide layer, bolstering the coating's ability to withstand wear-induced stresses. Furthermore, oxide particles can impart desirable biocompatible characteristics to the coating, aligning with the stringent requirements of orthopedic applications [174]. Al_2O_3, recognized for its exceptional hardness and corrosion resistance, plays a pivotal role in reinforcing PEO coatings for magnesium implants. Moreover, the integration of Al_2O_3 particles significantly boosts the coating's hardness, providing a robust defense against abrasive wear. This heightened hardness not only minimizes material loss during mechanical stresses, but also contributes to corrosion protection by forming a stable oxide layer [176–178]. Similarly, TiO_2, known for its biocompatibility and stabilizing effects, is a key component in tailoring PEO coatings for magnesium implants. When TiO_2 particles are incorporated into the coating, they enhance the biocompatibility of the surface, fostering a harmonious interaction with biological tissues. In addition, TiO_2 contributes to the formation of a stable oxide layer on the magnesium surface, bolstering wear resistance by acting as a protective barrier against abrasive wear. This dual functionality positions TiO_2 as a valuable choice for optimizing the longevity and performance of magnesium implants [198]. Likewise, ZrO_2, characterized by its high hardness and toughness, adds a robust dimension to PEO coatings. The inclusion of ZrO_2 particles enhances the coating's resistance to abrasive wear, providing a formidable defense against mechanical stresses. ZrO_2-reinforced coatings have shown promise in improving the durability of magnesium implants, especially in

load-bearing applications [179–181]. Similarly, CeO_2, with its unique combination of high hardness and self-healing properties, contributes to the wear resistance of PEO coatings. The self-healing nature of CeO_2 can mitigate the surface damage caused by abrasive wear, potentially extending the service life of magnesium implants [182,199]. This makes CeO_2 a compelling candidate for enhancing the longevity of orthopedic devices. In investigating the wear mechanism of CeO_2-incorporated PEO coatings on AM50 magnesium alloy substrates, the worn surfaces of steel ball counterparts were examined via SEM, as shown in Figure 11a–f [182]. The analysis revealed flattened surfaces for all balls against PEO coatings, confirming abrasive wear. Deep scoring indicated debris entrapment between the damaged coating and the ball. The steel ball hardness was approximately 900 HV. Testing against PEO-CeO_2 at a 10 N load showed a different wear mechanism compared with PEO alone (Figure 11g). Extensive plowing and debris detachment occurred, with fewer and shallower scores on balls sliding against PEO-CeO_2, suggesting that abrasive wear prevailed over the adhesive mechanism. Coating wear behavior against AISI 52100 steel balls was assessed, and COF versus distance was recorded for 2 N, 5 N, and 10 N loads (Figure 11g,h). Both coatings exhibited similar COF curve shapes at 2 N and 5 N, with COF stabilizing after initial fluctuations. At 10 N, distinct differences emerged. For the CeO_2-free coating, significant COF fluctuations occurred after 20 minutes, followed by a drop to ≈0.35, indicating coating failure. In contrast, PEO-CeO_2 reduced dynamic COF fluctuations, possibly due to debris filling pores, increasing the contact area, and contributing to elevated COF at higher loads. Additionally, YSZ, a stabilized form of ZrO_2 with yttrium oxide as the stabilizing agent, offers exceptional hardness and resistance to thermal and mechanical stresses. Incorporating YSZ particles into PEO coatings imparts improved wear resistance and thermal stability [200]. This is particularly advantageous in applications where implants may experience varying temperatures and mechanical loads. Furthermore, SiO_2 nanoparticles, characterized by their high hardness and biocompatibility, present an intriguing option for PEO coatings on magnesium implants. The addition of SiO_2 contributes to wear resistance while maintaining favorable interactions with biological tissues. This dual functionality positions silica as a versatile candidate for enhancing both the mechanical and biocompatible aspects of magnesium implant coatings [149,179]. Lastly, the incorporation of rare earth oxides, such as La_2O_3, introduces unique properties to PEO coatings. These oxides, known for their high hardness and corrosion resistance, enhance the coating's ability to withstand wear in aggressive environments. The addition of rare earth oxides presents opportunities for tailoring coatings to specific biomedical applications with stringent wear and corrosion requirements [92].

The inclusion of carbide particles elevates the PEO coating to unprecedented levels of hardness and wear resistance. Furthermore, the inherent toughness of carbide-reinforced coatings provides a robust defense against abrasive wear, making them particularly suited for applications where implants encounter challenging mechanical conditions. Moreover, carbide particles contribute to the formation of a wear-resistant surface, ensuring a sustained performance under cyclic loading and abrasive environments [201]. SiC, renowned for its exceptional hardness and abrasion resistance, is a stalwart choice for reinforcing PEO coatings. In addition, the inclusion of SiC particles significantly elevates the coating's ability to withstand abrasive wear, providing a formidable defense against mechanical stresses. Additionally, SiC-reinforced coatings have demonstrated promise in improving the longevity and durability of magnesium implants, especially in load-bearing scenarios where wear resistance is paramount [184–188]. WC, celebrated for its hardness and toughness, adds a robust dimension to PEO coatings on magnesium implants. Moreover, the incorporation of WC particles enhances the coating's resistance to abrasive wear, offering formidable protection against mechanical stresses. Similarly, WC-reinforced coatings exhibit substantial potential in augmenting the wear performance and structural integrity of magnesium implants, particularly in applications where the implants are subjected to dynamic loads and challenging environmental conditions [189–191]. TiC, known for its high hardness and wear resistance, is a valuable addition to PEO coatings. Additionally,

the incorporation of TiC particles enhances the coating's ability to withstand abrasive wear, providing a robust defense against mechanical stresses [202]. Furthermore, TiC-reinforced coatings showcase promise in improving the wear resistance and overall performance of magnesium implants, particularly in applications where hardness and durability are critical considerations [203]. Cr_3C_2, recognized for its high hardness and corrosion resistance, contributes significantly to wear resistance in PEO coatings. Similarly, the inclusion of Cr_3C_2 particles enhances the coating's ability to resist abrasive wear, providing a robust defense against mechanical stresses. In addition, Cr_3C_2-reinforced coatings demonstrate promise in enhancing the longevity and wear performance of magnesium implants, especially in environments where corrosion resistance is as crucial as wear resistance [204].

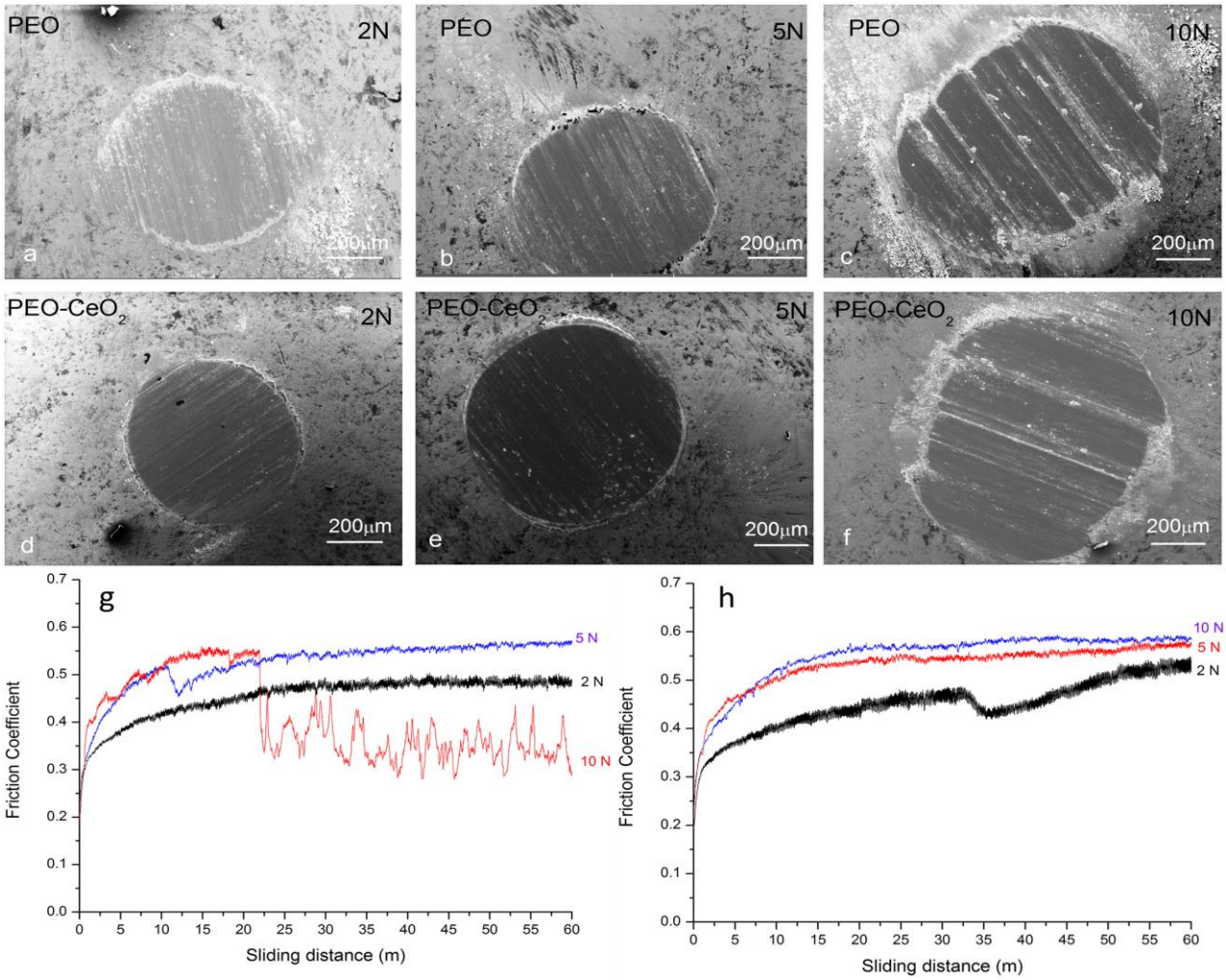

Figure 11. (**a**–**f**) Surface morphology of the steel ball counterparts slid against coated specimens under different loads of 2 N, 5 N, and 10 N. Variation of friction coefficient with sliding distance for (**g**) PEO and (**h**) PEO-CeO_2 coatings under 2 N, 5 N, and10 N loads. Figure adapted with permission from [182].

Incorporating nitrided particles into PEO coatings for magnesium implants offers a unique avenue for enhancing wear resistance and corrosion protection [192]. Nitrided particles, typically compounds containing nitrogen, introduce distinct mechanical and electrochemical properties to the coatings, contributing to their overall performance in challenging biomedical environments [193]. TiN is a notable example of a nitrided particle that has shown promise in reinforcing PEO coatings. Known for its high hardness and excellent wear resistance, TiN particles enhance the coating's ability to withstand abrasive wear and mechanical stresses. The incorporation of TiN contributes to the overall durability

of magnesium implants, particularly in load-bearing applications where wear resistance is crucial [192–194]. Si_3N_4 is recognized for its exceptional toughness, high-temperature stability, and corrosion resistance. The incorporation of Si_3N_4 particles into PEO coatings can contribute to enhanced mechanical properties, wear resistance, and corrosion protection. Si_3N_4-reinforced coatings may offer a comprehensive solution to the challenges associated with the dynamic biomechanical environment of magnesium implants [205].

The incorporation of MoS_2 and WS_2 particles into PEO coatings for magnesium implants introduces a fascinating dimension to enhance wear resistance and lubrication properties. These transition metal dichalcogenides exhibit unique structural and tribological characteristics that can significantly impact the performance of PEO-coated magnesium surfaces. MoS_2 is renowned for its lamellar structure and inherent lubricating properties. When integrated into PEO coatings, MoS_2 particles provide a solid lubricating layer, reducing friction between moving parts. This lubricity contributes to improved wear resistance by minimizing material loss during sliding or cyclic motion. MoS_2-reinforced coatings present an intriguing avenue for applications where low friction and enhanced wear resistance are paramount. Similar to MoS_2, WS_2 possesses a layered structure with excellent lubricating characteristics. When incorporated into PEO coatings, WS_2 particles contribute to reduced friction and enhanced wear resistance. The lamellar arrangement of WS_2 particles forms a boundary-lubricating film, offering protection against abrasive wear and reducing the risk of surface damage. WS_2-reinforced coatings hold promise in scenarios where sustained lubrication is critical for the long-term functionality of magnesium implants [195].

Graphite, renowned for its superior lubricating properties, is a pivotal element in magnesium-implant PEO coatings. The introduction of graphite particles revolutionizes these coatings' tribological dynamics, enhancing wear resistance in orthopedic applications [206]. Graphite's hexagonal lattice structure enables the formation of a self-renewing lubricating film in PEO coatings, reducing friction and preventing direct metal-to-metal contact. This film acts as a protective shield during mechanical interactions, significantly reducing wear and surface damage. In load-bearing applications, such as joint implants, graphite-infused PEO coatings ensure prolonged durability and functionality [194]. The unique lubrication mechanism of graphite makes it particularly appealing for orthopedic scenarios where minimizing friction is crucial for preventing wear-related issues and complications. The combination of graphite with other reinforcing particles may further enhance the mechanical strength, corrosion resistance, and tailored tribological properties, offering a comprehensive solution for optimizing magnesium-implant performance [194,206]. Graphene particles also play a crucial role in enhancing wear resistance in PEO coatings by showcasing exceptional mechanical strength and unique lubricating properties. Their incorporation forms a reinforcing network, providing an additional defense against wear challenges [196]. Furthermore, the two-dimensional structure of graphene contributes to coating flexibility, minimizing the risk of cracking. This outstanding mechanical strength of graphene fortifies PEO coatings, reducing material loss and improving the durability of magnesium implants, especially in abrasive scenarios [207]. Moreover, graphene not only reduces friction, but also lowers wear rates during motion, benefiting orthopedic implants by preventing accelerated wear and potential tissue complications. The thermal conductivity of graphene efficiently dissipates frictional heat, ensuring implant stability in the dynamic biomechanical environment of the human body [207,208]. Its flexibility allows it to conform to the substrate, thereby reducing the risk of coating cracking or delamination. Additionally, graphene's biocompatibility supports favorable interactions with biological tissues, which is crucial for the integration and acceptance of magnesium implants within the human body [208]. Moving on to the experimental results, Figure 12a illustrates the friction coefficient evolution during sliding for test specimens [209]. Initially (Stage I), all specimens experienced a rapid increase, followed by stabilization (Stage II). Notably, the Mg-Li alloy showed lower friction due to a smooth surface, but prolonged sliding resulted in higher coefficients ($\approx$0.52). In contrast, coatings with graphene oxide

(GO) exhibited lower coefficients (≈0.28, ≈0.12) attributed to fewer micro-pores, higher hardness, compactness, and elemental C presence, enhancing the tribological performance. The relationship between wear track depths/volumes and their 3D topographies was apparent in the as-prepared coatings, showing a significant decrease in both wear width and wear depth compared with the substrate [209]. The GO-containing coating, in particular, demonstrated the most substantial reduction, as illustrated in Figure 12b. Moving on to Figure 12c, which illustrates the abrasion process of the PEO coatings in a schematic manner, it is evident that in the initial stage (Stage I), the dominant model was the "steel-on-protrusions", emphasizing abrasive wear. During this stage, friction coefficients increased rapidly as the real contact areas expanded, leading to the transfer of wear debris from the stainless-steel ball onto the coating [209]. As sliding progressed (Stage II), asperities wore out, debris entered the micro-pores, and stable friction coefficients were observed. At elevated temperatures, severe adhesive wear became prominent. The performance in terms of friction and wear was influenced by the presence of lubricating materials and hard particles for antifriction, as well as the coating's hardness, thickness, and roughness for wear resistance. The coating containing GO exhibited lower roughness, higher hardness, and greater compactness, contributing to improved tribological behavior. Despite the presence of elemental carbon on the wear trace, the fine debris in the micro-pores played a role in influencing wear performance [209].

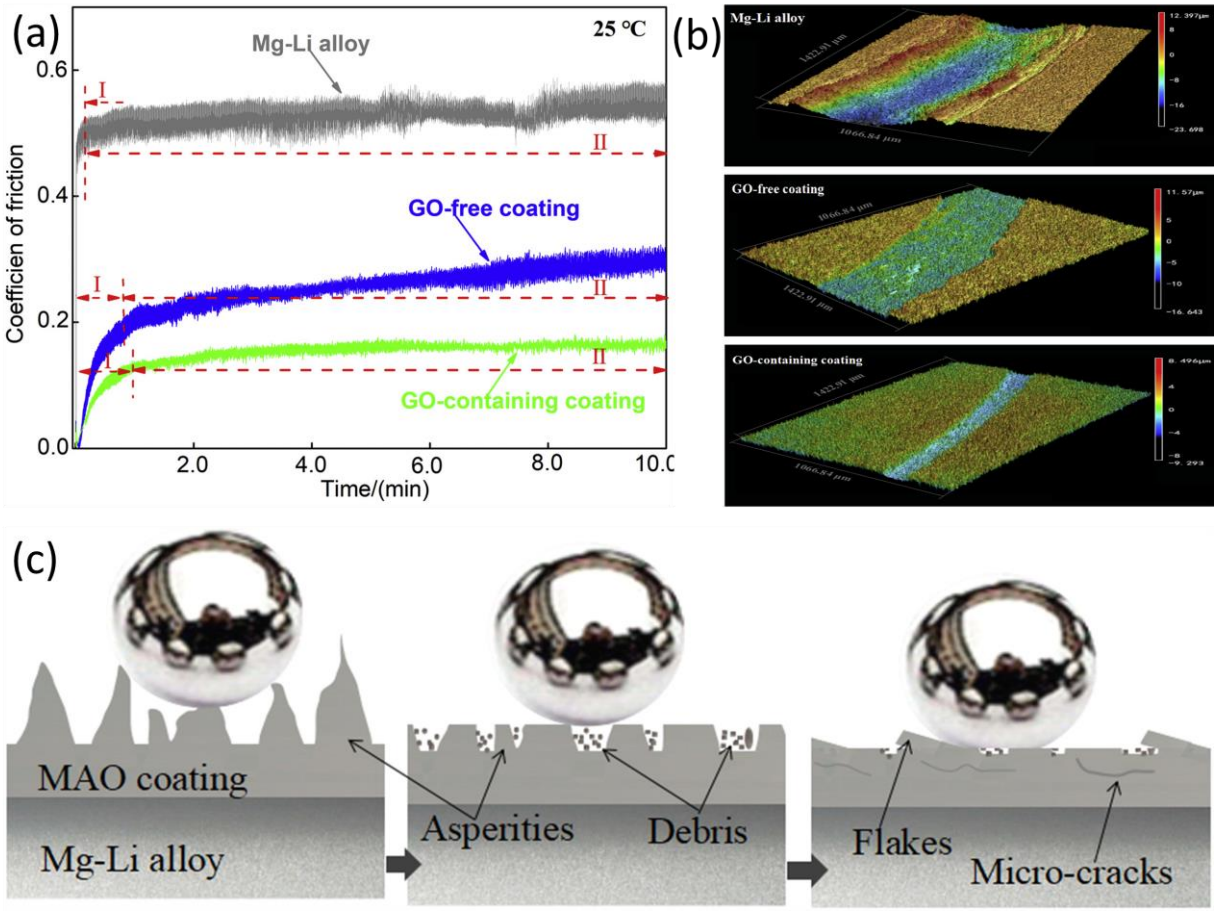

Figure 12. (**a**) Changes in friction coefficients for the specimens at varying temperatures, (**b**) three-dimensional topographies of wear tracks post-wear tests, and (**c**) a diagrammatic representation of the wear mechanism for the PEO (alternatively known as MAO) coating. Figure adapted with permission from [209].

9. Conclusions and Future Directions

As a comprehensive review of the existing literature in this field, the following key conclusions can be drawn:

- Magnesium alloys are highly promising biomaterials in biomedical engineering due to their osteoconductive and antibacterial properties.
- However, their accelerated corrosion in body fluids compromises their mechanical integrity and can impede healing.
- Surface coating and alloying techniques have effectively mitigated magnesium's corrosion rate, with the plasma electrolytic oxidation (PEO) process proving successful.
- PEO coatings have limitations, including microcracks and pores, that restrict their corrosion resistance.
- Incorporating particles into PEO coatings on magnesium implants effectively enhances the surface morphology, microstructure, and electrochemical properties.
- Modifying electrolyte conditions based on particle presence can reduce porosities and improve coating properties, although achieving uniform particle dispersion can be challenging.
- Zeta potential analysis indicates that most nanoparticles in PEO procedures have a negative charge in common alkaline electrolytes, encouraging their incorporation into the coating.
- Incorporating particles and sealing existing pores modify the coating's surface structure, resulting in increased corrosion resistance.
- The likelihood of particle incorporation is determined by using high temperature and discharge pressure and by considering particle characteristics.
- PEO coatings on magnesium and its alloys can benefit significantly from adding nano and microparticles to electrolytes, altering the phase composition, microstructure, thickness, and corrosion properties.
- Introducing particles reduces the porosity in PEO coatings, thus improving their microstructure by filling and sealing the micropores.
- Enhanced microstructure prevents destructive ion penetration from the coating into the substrate, contributing to improved corrosion resistance.
- The addition of particles to electrolytes not only influences the thickness and roughness, but also enhances the hydrophobicity of the coating.

There are numerous promising avenues for advancing research and exploration in enhancing magnesium alloy performance through innovative coating techniques. While prior studies have delved into incorporating various particles into PEO coatings on magnesium and its alloys, there has been a noticeable scarcity of research about their corrosion-resistance properties. We anticipate that future investigations will provide heightened attention to this crucial aspect. Further exploration is imperative to gain insight into the diverse effects of different particles on PEO coatings for magnesium and its alloys, considering the impact of particle size and intrinsic properties, particularly concerning corrosion resistance. Additionally, numerous oxide particles, such as strontium oxide, manganese oxide, calcium oxide, potassium oxide, tantalum oxide, and copper oxide, which exhibit a high bioactivity and desired osteoconductivity, have yet to be thoroughly examined within the context of PEO coatings for magnesium implants. Future research in this field should also explore the long-term corrosion behavior of particle-incorporated PEO coatings on magnesium alloys in simulated body fluids, addressing a critical aspect for assessing their suitability for extended implant applications.

In addition to the significant strides that will be gained in understanding the corrosion behavior of PEO coatings on magnesium implants with particle incorporation, it is crucial to address the implications for wear resistance. While much attention has rightfully been devoted to mitigating corrosion challenges, the interplay between particle-enhanced PEO coatings and wear characteristics holds immense importance in the realm of implant performance. Future investigations should delve into the wear behavior of these coatings, exploring how the introduced particles influence friction, material loss, and mechanical sta-

bility over extended usage. Moreover, striking a balance between enhanced wear resistance and maintaining other crucial coating properties poses an ongoing challenge. Understanding the synergistic effects of particle addition on both corrosion and wear resistance will be pivotal for advancing the overall durability and functionality of magnesium implants in orthopedic applications.

Author Contributions: Y.Q.A.—conceptualization, methodology, and writing (original draft preparation); E.A.—resources and writing (original draft preparation); M.F.J.—software, writing (original draft preparation); L.H.S. methodology, writing (original draft preparation); S.A.—writing (original draft preparation), funding acquisition; S.A.Z.—resources and writing (original draft preparation); A.F.A.—software, writing (original draft preparation), supervision; A.A.—writing (review and editing); F.S.—writing (review and editing) and supervision; M.S.B.—writing (review and editing) and supervision. All authors have read and agreed to the published version of the manuscript.

Funding: This research received no external funding.

Data Availability Statement: Not applicable.

Conflicts of Interest: The authors declare no conflict of interest.

References

1. Alshimaysawee, S.; Fadhel Obaid, R.; Al-Gazally, M.E.; Alexis Ramírez-Coronel, A.; Bathaei, M.S. Recent Advancements in Metallic Drug-Eluting Implants. *Pharmaceutics* **2023**, *15*, 223. [CrossRef] [PubMed]
2. Bazli, L.; Nargesi Khoramabadi, H.; Modarresi Chahardehi, A.; Arsad, H.; Malekpouri, B.; Asgari Jazi, M.; Azizabadi, N. Factors influencing the failure of dental implants: A systematic review. *J. Compos. Compd.* **2020**, *2*, 18–25. [CrossRef]
3. Ghazanfari, H.; Hasanizadeh, S.; Eskandarinezhad, S.; Hassani, S.; Sheibani, M.; Torkamani, A.D.; Fakić, B. Recent progress in materials used towards corrosion protection of Mg and its alloys. *J. Compos. Compd.* **2020**, *2*, 205–214. [CrossRef]
4. Zhu, W.Y.; Guo, J.; Yang, W.F.; Tao, Z.Y.; Lan, X.; Wang, L.; Xu, J.; Qin, L.; Su, Y.X. Biodegradable magnesium implant enhances angiogenesis and alleviates medication-related osteonecrosis of the jaw in rats. *J. Orthop. Transl.* **2022**, *33*, 153–161. [CrossRef]
5. Espiritu, J.; Meier, M.; Seitz, J.M. The current performance of biodegradable magnesium-based implants in magnetic resonance imaging: A review. *Bioact. Mater.* **2021**, *6*, 4360–4367. [CrossRef] [PubMed]
6. Niazvand, F.; Cheshmi, A.; Zand, M.; NasrAzadani, R.; Kumari, B.; Raza, A.; Nasibi, S. An overview of the development of composites containing Mg and Zn for drug delivery. *J. Compos. Compd.* **2020**, *2*, 193–204. [CrossRef]
7. Fard, M.G.; Sharifianjazi, F.; Kazemi, S.S.; Rostamani, H.; Bathaei, M.S. Laser-Based Additive Manufacturing of Magnesium Alloys for Bone Tissue Engineering Applications: From Chemistry to Clinic. *J. Manuf. Mater. Process.* **2022**, *6*, 158. [CrossRef]
8. Koopaie, M.; Bordbar-Khiabani, A.; Kolahdooz, S.; Darbandsari, A.K.; Mozafari, M. Advanced surface treatment techniques counteract biofilm-associated infections on dental implants. *Mater. Res. Express* **2020**, *7*, 015417. [CrossRef]
9. Ma, H. Research on promotion of lower limb movement function recovery after stroke by using lower limb rehabilitation robot in combination with constant velocity muscle strength training. In Proceedings of the IEEE 2021 7th International Symposium on Mechatronics and Industrial Informatics (ISMII), Zhuhai, China, 22–24 January 2021; pp. 70–73.
10. Li, D.; Zhang, D.; Yuan, Q.; Liu, L.; Li, H.; Xiong, L.; Guo, X.; Yan, Y.; Yu, K.; Dai, Y.; et al. In vitro and in vivo assessment of the effect of biodegradable magnesium alloys on osteogenesis. *Acta Biomater.* **2022**, *141*, 454–465. [CrossRef]
11. Haowei, M.A.; Hussein, U.A.; Al-Qaim, Z.H.; Altalbawy, F.M.; Fadhil, A.A.; Al-Taee, M.M.; Hadrawi, S.K.; Khalaf, R.M.; Jirjees, I.H.; Zarringhalam, M.; et al. Employing Sisko non-Newtonian model to investigate the thermal behavior of blood flow in a stenosis artery: Effects of heat flux, different severities of stenosis, and different radii of the artery. *Alex. Eng. J.* **2023**, *68*, 291–300. [CrossRef]
12. Al-Alwany, A. Latrogenic atrial septal defect post radiofrequency ablation in patients with left atrial SVT: Predictors and outcomes. *Rev. Latinoam. Hipertens.* **2021**, *16*, 185–191.
13. Al Alwany, A.A. Effect and benefit of percutaneous coronary intervention in chronic total occlusion on ventricular repolarization: QT correction and dispersion. *J. Med. Life* **2022**, *15*, 1025. [CrossRef] [PubMed]
14. Singh, N.; Batra, U.; Kumar, K.; Ahuja, N.; Mahapatro, A. Progress in bioactive surface coatings on biodegradable Mg alloys: A critical review towards clinical translation. *Bioact. Mater.* **2023**, *19*, 717–757. [CrossRef] [PubMed]
15. Zamani, Y.; Ghazanfari, H.; Erabi, G.; Moghanian, A.; Fakić, B.; Hosseini, S.M.; Mahammod, B.P. A review of additive manufacturing of Mg-based alloys and composite implants. *J. Compos. Compd.* **2021**, *3*, 71–83. [CrossRef]
16. Altaher, Y.; Kandeel, M. Structure-Activity Relationship of Anionic and Cationic Polyamidoamine (PAMAM) Dendrimers against Staphylococcus aureus. *J. Nanomater.* **2022**, *2022*, 4013016. [CrossRef]
17. Hjazi, A. The effects of Capsicum annuum supplementation on lipid profiles in adults with metabolic syndrome and related disorders: A systematic review and meta-analysis of randomized controlled trials. *Phytother. Res.* **2023**, *37*, 3859–3866. [CrossRef] [PubMed]

18. Zerankeshi, M.M.; Alizadeh, R.; Gerashi, E.; Asadollahi, M.; Langdon, T.G. Effects of heat treatment on the corrosion behavior and mechanical properties of biodegradable Mg alloys. *J. Magnes. Alloy.* **2022**, *10*, 1737–1785. [CrossRef]
19. Sahu, M.R.; Kumar, T.S.; Chakkingal, U. A review on recent advancements in biodegradable Mg-Ca alloys. *J. Magnes. Alloy.* **2022**, *10*, 2094–2117. [CrossRef]
20. Tsakiris, V.; Tardei, C.; Clicinschi, F.M. Biodegradable Mg alloys for orthopedic implants—A review. *J. Magnes. Alloy.* **2021**, *9*, 1884–1905. [CrossRef]
21. Kasaeian-Naeini, M.; Sedighi, M.; Hashemi, R. Severe plastic deformation (SPD) of biodegradable magnesium alloys and composites: A review of developments and prospects. *J. Magnes. Alloy.* **2022**, *10*, 938–955. [CrossRef]
22. Al Alwany, A.A. Echocardiographic assessment of the aortic stenosis valve area: Parameters and outcome. *J. Med. Chem. Sci.* **2022**, *3*, 2D. [CrossRef]
23. Sampatirao, H.; Radhakrishnapillai, S.; Dondapati, S.; Parfenov, E.; Nagumothu, R. Developments in plasma electrolytic oxidation (PEO) coatings for biodegradable magnesium alloys. *Mater. Today Proc.* **2021**, *46*, 1407–1415. [CrossRef]
24. Zamani, Y.; Zareein, A.; Bazli, L.; NasrAzadani, R.; Mahammod, B.P.; Nasibi, S.; Chahardehi, A.M. Nanodiamond-containing composites for tissue scaffolds and surgical implants: A review. *J. Compos. Compd.* **2020**, *2*, 215–227. [CrossRef]
25. Xie, K.; Wang, N.; Guo, Y.; Zhao, S.; Tan, J.; Wang, L.; Li, G.; Wu, J.; Yang, Y.; Xu, W.; et al. Additively manufactured biodegradable porous magnesium implants for elimination of implant-related infections: An in vitro and in vivo study. *Bioact. Mater.* **2022**, *8*, 140–152. [CrossRef] [PubMed]
26. Xie, K.; Wang, L.; Guo, Y.; Zhao, S.; Yang, Y.; Dong, D.; Ding, W.; Dai, K.; Gong, W.; Yuan, G.; et al. Effectiveness and safety of biodegradable Mg-Nd-Zn-Zr alloy screws for the treatment of medial malleolar fractures. *J. Orthop. Transl.* **2021**, *27*, 96–100. [CrossRef] [PubMed]
27. Sekar, P.; Narendranath, S.; Desai, V. Recent progress in in vivo studies and clinical applications of magnesium based biodegradable implants—A review. *J. Magnes. Alloy.* **2021**, *9*, 1147–1163. [CrossRef]
28. Istrate, B.; Munteanu, C.; Antoniac, I.V.; Lupescu, Ș.C. Current research studies of Mg–Ca–Zn biodegradable alloys used as orthopedic implants. *Crystals* **2022**, *12*, 1468. [CrossRef]
29. Chow, D.H.; Wang, J.; Wan, P.; Zheng, L.; Ong, M.T.; Huang, L.; Tong, W.; Tan, L.; Yang, K.; Qin, L. Biodegradable magnesium pins enhanced the healing of transverse patellar fracture in rabbits. *Bioact. Mater.* **2021**, *6*, 4176–4185. [CrossRef]
30. Zehra, T.; Fattah-alhosseini, A.; Kaseem, M. Surface properties of plasma electrolytic oxidation coating modified by polymeric materials: A review. *Prog. Org. Coat.* **2022**, *171*, 107053. [CrossRef]
31. Zehra, T.; Kaseem, M. Recent advances in surface modification of plasma electrolytic oxidation coatings treated by non-biodegradable polymers. *J. Mol. Liq.* **2022**, *365*, 120091. [CrossRef]
32. Zhi, P.; Liu, L.; Chang, J.; Liu, C.; Zhang, Q.; Zhou, J.; Liu, Z.; Fan, Y. Advances in the study of magnesium alloys and their use in bone implant material. *Metals* **2022**, *12*, 1500. [CrossRef]
33. Jia, P.; Pan, Y.; Yu, L.; Wang, J.; Feng, R.; Wang, Y.; Fang, X.; Chen, C. In vitro degradation and corrosion evaluations of plasma electrolytic oxidized Mg–Zn–Ca–Si alloys for biomedical applications. *J. Mater. Res. Technol.* **2023**, *23*, 2410–2425. [CrossRef]
34. Zhang, Y.; Li, Y.; Lv, Y.; Zhang, X.; Dong, Z.; Yang, L.; Zhang, E. Ag distribution and corrosion behaviour of the plasma electrolytic oxidized antibacterial Mg-Ag alloy. *Electrochim. Acta* **2022**, *411*, 140089. [CrossRef]
35. Ali, W.; Li, M.; Tillmann, L.; Mayer, T.; González, C.; LLorca, J.; Kopp, A. Bioabsorbable WE43 Mg alloy wires modified by continuous plasma-electrolytic oxidation for implant applications. Part I: Processing, microstructure and mechanical properties. *Biomater. Adv.* **2023**, *146*, 213314. [CrossRef] [PubMed]
36. Mashtalyar, D.V.; Nadaraia, K.V.; Plekhova, N.G.; Imshinetskiy, I.M.; Piatkova, M.A.; Pleshkova, A.I.; Kislova, S.E.; Sinebryukhov, S.L.; Gnedenkov, S.V. Antibacterial Ca/P-coatings formed on Mg alloy using plasma electrolytic oxidation and antibiotic impregnation. *Mater. Lett.* **2022**, *317*, 132099. [CrossRef]
37. Kopp, A.; Fischer, H.; Soares, A.P.; Schmidt-Bleek, K.; Leber, C.; Kreiker, H.; Duda, G.; Kröger, N.; van Gaalen, K.; Hanken, H.; et al. Long-term in vivo observations show biocompatibility and performance of ZX00 magnesium screws surface-modified by plasma-electrolytic oxidation in Göttingen miniature pigs. *Acta Biomater.* **2023**, *157*, 720–733. [CrossRef]
38. Chen, S.S.; Song, P.D.; Yin, J.; Qi, K.; Li, H.D.; Hou, L.; Li, W.H. Enhancement of Plasticity and Biocorrosion Resistance in a Plasma Electrolytic Oxidation-Treated Mg-Based Amorphous Alloy Composite. *J. Mater. Eng. Perform.* **2023**, *32*, 2298–2306. [CrossRef]
39. Yu, K.; Li, P.; Han, Q.; Wang, Q.; Karpushenkov, S.A.; Lu, X.; Ignatenko, O.V. Investigation of biodegradability, cytocompatibility and antibacterial property of plasma electrolytic oxidation coating on Mg. *Surf. Interfaces* **2022**, *30*, 101840. [CrossRef]
40. Shishir, R.; Lokeshkumar, E.; Manojkumar, P.; Nasiruddin, U.; Premchand, C.; Ponnilavan, V.; Rameshbabu, N. Development of biocompatible and corrosion-resistant plasma electrolytic oxidation coating over zinc for orthopedic implant applications. *Surf. Coat. Technol.* **2022**, *450*, 128990.
41. Bordbar-Khiabani, A.; Ebrahimi, S.; Yarmand, B. Highly corrosion protection properties of plasma electrolytic oxidized titanium using rGO nanosheets. *Appl. Surf. Sci.* **2019**, *486*, 153–165. [CrossRef]
42. Chen, Z.; Liu, X.; Cheng, Z.; Tan, X.; Xiang, Y.; Li, J.; Zhang, Y.; Lu, Z.; Kang, E.T.; Xu, L.; et al. Degradation behavior, biocompatibility and antibacterial activity of plasma electrolytic oxidation treated zinc substrates. *Surf. Coat. Technol.* **2023**, *455*, 129234. [CrossRef]
43. Wei, L.; Gao, Z. Recent research advances on corrosion mechanism and protection, and novel coating materials of magnesium alloys: A review. *RSC Adv.* **2023**, *13*, 8427–8463. [CrossRef] [PubMed]

44. Wang, L.; He, J.; Yu, J.; Arthanari, S.; Lee, H.; Zhang, H.; Lu, L.; Huang, G.; Xing, B.; Wang, H.; et al. Degradable Magnesium Corrosion Control for Implant Applications. *Materials* **2022**, *15*, 6197. [CrossRef] [PubMed]
45. Xu, L.; Liu, X.; Sun, K.; Fu, R.; Wang, G. Corrosion Behavior in Magnesium-Based Alloys for Biomedical Applications. *Materials* **2022**, *15*, 2613. [CrossRef] [PubMed]
46. Kumar, S.; Katyal, P.; Chaudhary, R.N.; Singh, V. Assessment of factors influencing bio-corrosion of magnesium based alloy implants: A review. *Mater. Today Proc.* **2022**, *56*, 2680–2689. [CrossRef]
47. van Gaalen, K.; Quinn, C.; Benn, F.; McHugh, P.E.; Kopp, A.; Vaughan, T.J. Linking the effect of localised pitting corrosion with mechanical integrity of a rare earth magnesium alloy for implant use. *Bioact. Mater.* **2023**, *21*, 32–43. [CrossRef]
48. Kim, J.; Pan, H. Effects of magnesium alloy corrosion on biological response-Perspectives of metal-cell interaction. *Prog. Mater. Sci.* **2022**, *133*, 101039. [CrossRef]
49. Kumarm, D.; Jain, J.; Gosvami, N.N. Macroscale to nanoscale tribology of magnesium-based alloys: A review. *Tribol. Lett.* **2022**, *70*, 27. [CrossRef]
50. Shen, G.; Fang, F.; Kang, C. Tribological performance of bioimplants: A comprehensive review. *J. NPE* **2018**, *1*, 107–122.
51. Deepak, J.R.; Joy, N.; Arunkumar, T.; Srivatsan, R.; Gnanasekar, R. Tribological investigation of magnesium rare earth alloy for orthopedic application. *Mater. Today Proc.* **2021**, *47*, 4767–4771. [CrossRef]
52. Ghanbari, A.; Khiabani, A.B.; Zamanian, A.; Yarmand, B.; Mozafari, M. The competitive mechanism of plasma electrolyte oxidation for the formation of magnesium oxide bioceramic coatings. *Mater. Today Proc.* **2018**, *5*, 15677–15685. [CrossRef]
53. Bordbar-Khiabani, A.; Yarmand, B.; Mozafari, M. Emerging magnesium-based biomaterials for orthopedic implantation. *Emerg. Mater. Res.* **2020**, *8*, 305–319. [CrossRef]
54. Darband, G.B.; Aliofkhazraei, M.; Hamghalam, P.; Valizade, N. Plasma electrolytic oxidation of magnesium and its alloys: Mechanism, properties and applications. *J. Magnes. Alloy.* **2017**, *5*, 74–132. [CrossRef]
55. Khiabani, A.B.; Ghanbari, A.; Yarmand, B.; Zamanian, A.; Mozafari, M. Improving corrosion behavior and in vitro bioactivity of plasma electrolytic oxidized AZ91 magnesium alloy using calcium fluoride containing electrolyte. *Mater. Lett.* **2018**, *212*, 98–102. [CrossRef]
56. Asgari, M.; Daneshmand, H.; Darband, G.B.; Rouhaghdam, A.S. Single-stage production of glass sealed PEO composite coating on AZ31B. *Surf. Interfaces* **2020**, *21*, 100712. [CrossRef]
57. Yao, W.; Wu, L.; Wang, J.; Jiang, B.; Zhang, D.; Serdechnova, M.; Shulha, T.; Blawert, C.; Zheludkevich, M.L.; Pan, F. Micro-arc oxidation of magnesium alloys: A review. *J. Mater. Sci. Technol.* **2022**, *118*, 158–180. [CrossRef]
58. Jin, S.; Ma, X.; Wu, R.; Wang, G.; Zhang, J.; Krit, B.; Betsofen, S.; Liu, B. Advances in micro-arc oxidation coatings on Mg-Li alloys. *Appl. Surf. Sci. Adv.* **2022**, *8*, 100219. [CrossRef]
59. Chen, Y.; Wu, L.; Yao, W.; Wu, J.; Yuan, Y.; Xie, Z.; Jiang, B.; Pan, F. Synergistic effect of graphene oxide/ternary Mg-Al-La layered double hydroxide for dual self-healing corrosion protection of micro-arc oxide coating of magnesium alloy. *Colloids Surf. A Physicochem. Eng. Asp.* **2022**, *655*, 130339. [CrossRef]
60. Askarnia, R.; Fardi, S.R.; Sobhani, M.; Staji, H.; Aghamohammadi, H. Effect of graphene oxide on properties of AZ91 magnesium alloys coating developed by micro-arc oxidation process. *J. Alloys Compd.* **2022**, *892*, 162106. [CrossRef]
61. Chen, Y.; Wu, L.; Yao, W.; Wu, J.; Yuan, Y.; Jiang, B.; Pan, F. Growth behavior and corrosion resistance of graphene oxide/MgAl Layered double hydroxide coating grown on micro-arc oxidation film of magnesium alloys. *J. Ind. Eng. Chem.* **2023**, *117*, 319–332. [CrossRef]
62. Yang, S.; Wang, C.; Li, F.; Liu, N.; Shi, P.; Wang, B.; Sun, R. One-step in situ growth of a simple and efficient pore-sealing coating on micro-arc oxidized AZ31B magnesium alloy. *J. Alloys Compd.* **2022**, *909*, 164710. [CrossRef]
63. Pesode, P.; Barve, S.; Mane, Y.; Dayane, S.; Kolekar, S.; Mohammed, K.A. Recent advances on biocompatible coating on magnesium alloys by micro arc oxidation technique. *Key Eng. Mater.* **2023**, *944*, 117–134. [CrossRef]
64. Chen, Y.; Wu, L.; Yao, W.; Chen, Y.; Zhong, Z.; Ci, W.; Wu, J.; Xie, Z.; Yuan, Y.; Pan, F. A self-healing corrosion protection coating with graphene oxide carrying 8-hydroxyquinoline doped in layered double hydroxide on a micro-arc oxidation coating. *Corros. Sci.* **2022**, *194*, 109941. [CrossRef]
65. Li, T.; Zhao, Y.; Chen, M. Study on Enhancing the Corrosion Resistance and Photo-Thermal Antibacterial Properties of the Micro-Arc Oxidation Coating Fabricated on Medical Magnesium Alloy. *Int. J. Mol. Sci.* **2022**, *23*, 10708. [CrossRef] [PubMed]
66. Zhang, A.M.; Liu, C.; Sui, P.S.; Sun, C.; Cui, L.Y.; Kannan, M.B.; Zeng, R.C. Corrosion resistance and mechanisms of smart micro-arc oxidation/epoxy resin coatings on AZ31 Mg alloy: Strategic positioning of nanocontainers. *J. Magnes. Alloy.* **2023**. [CrossRef]
67. Ma, C.; Liu, J.; Zhang, Z.; Wu, F.; Wen, Y.; Shang, W. Preparation and Properties of Micro-Arc Oxidation/Self-Assembly Coatings with Different Hydrophobicities on Magnesium Alloy. *Adv. Eng. Mater.* **2022**, *24*, 2200741. [CrossRef]
68. Fattah-alhosseini, A.; Babaei, K.; Molaei, M. Plasma electrolytic oxidation (PEO) treatment of zinc and its alloys: A review. *Surf. Interfaces* **2020**, *18*, 100441. [CrossRef]
69. Xue, Y.; Pang, X.; Karparvarfard, S.M.; Jahed, H.; Luo, S.; Shen, Y. Corrosion Protection of ZK60 Wrought Magnesium Alloys by Micro-Arc Oxidation. *Metals* **2022**, *12*, 449. [CrossRef]
70. Chen, L.; Zhao, R.; Qi, H.; Chen, D.; Zhou, S.; Wang, X.; Li, W. Influence of voltage modes on microstructure and corrosion resistance of micro-arc oxidation coating on magnesium alloy. *J. Adhes. Sci. Technol.* **2023**, *37*, 2232–2246. [CrossRef]

71. Dong, H.; Li, Q.; Xie, D.; Jiang, W.; Ding, H.; Wang, S.; An, L. Forming characteristics and mechanisms of micro-arc oxidation coatings on magnesium alloys based on different types of single electrolyte solutions. *Ceram. Int.* **2023**, *49*, 32271–32281. [CrossRef]
72. Sun, H.; Wang, Y.; Sun, C.; Yu, H.; Xi, Z.; Liu, N.; Zhang, N. In vivo comparison of the degradation and osteointegration properties of micro-arc oxidation-coated Mg-Sr and Mg-Ca alloy scaffolds. *Bio-Med. Mater. Eng.* **2022**, *33*, 209–219. [CrossRef] [PubMed]
73. Chaharmahali, R.; Fattah-Alhosseini, A.; Nouri, M.; Babaei, K. Improving surface characteristics of PEO coatings of Mg and its alloys with zirconia nanoparticles: A review. *Appl. Surf. Sci. Adv.* **2021**, *6*, 100131. [CrossRef]
74. O'Hara, M.; Troughton, S.C.; Francis, R.; Clyne, T.W. The incorporation of particles suspended in the electrolyte into plasma electrolytic oxidation coatings on Ti and Al substrates. *Surf. Coat. Technol.* **2020**, *385*, 125354. [CrossRef]
75. Lu, X.; Mohedano, M.; Blawert, C.; Matykina, E.; Arrabal, R.; Kainer, K.U.; Zheludkevich, M.L. Plasma electrolytic oxidation coatings with particle additions—A review. *Surf. Coat. Technol.* **2016**, *307*, 1165–1182. [CrossRef]
76. Schwartz, A.; Kossenko, A.; Zinigrad, M.; Danchuk, V.; Sobolev, A. Cleaning Strategies of Synthesized Bioactive Coatings by PEO on Ti-6Al-4V Alloys of Organic Contaminations. *Materials* **2023**, *16*, 4624. [CrossRef] [PubMed]
77. Sobolev, A.; Kossenko, A.; Zinigrad, M.; Borodianskiy, K. Comparison of plasma electrolytic oxidation coatings on Al alloy created in aqueous solution and molten salt electrolytes. *Surf. Coat. Technol.* **2018**, *344*, 590–595. [CrossRef]
78. Sobolev, A.; Zinigrad, M.; Borodianskiy, K. Ceramic coating on Ti-6Al-4V by plasma electrolytic oxidation in molten salt: Development and characterization. *Surf. Coat. Technol.* **2021**, *408*, 126847. [CrossRef]
79. Jamali, R.; Bordbar-Khiabani, A.; Yarmand, B.; Mozafari, M.; Kolahi, A. Effects of co-incorporated ternary elements on biocorrosion stability, antibacterial efficacy, and cytotoxicity of plasma electrolytic oxidized titanium for implant dentistry. *Mater. Chem. Phys.* **2022**, *276*, 125436. [CrossRef]
80. Jin, X.; Mei, D.; Chen, D.; Li, Y.; Wang, L.; Zhu, S.; Guan, S. β-TCP particles additive synergistically improves corrosion resistance and biocompatibility of micro-arc oxide coated magnesium alloy. *Mater. Today Commun.* **2023**, *36*, 106694. [CrossRef]
81. Pourshadloo, M.; Rezaei, H.A.; Saeidnia, M.; Alkokab, H.; Bathaei, M.S. Effect of G-family incorporation on corrosion behavior of PEO-treated titanium alloys: A review. *Surf. Innov.* **2022**, *11*, 5–14. [CrossRef]
82. Amiri, M.; Padervand, S.; Targhi, V.T.; Khoei, S.M.M. Investigation of aluminum oxide coatings created by electrolytic plasma method in different potential regimes. *J. Compos. Compd.* **2020**, *2*, 115–122. [CrossRef]
83. Ma, X.; Jin, S.; Wu, R.; Zhang, S.; Hou, L.; Krit, B.; Betsofen, S.; Liu, B. Influence of combined B_4C/C particles on the properties of microarc oxidation coatings on Mg-Li alloy. *Surf. Coat. Technol.* **2022**, *438*, 128399. [CrossRef]
84. Selvi, E.; Kaba, M.; Muhaffel, F.; Serdar Vanlı, A.; Baydoğan, M. Elevated Temperature Wear Behavior of AZ91 Magnesium Alloy after Micro-Arc Oxidation in Single and Dual Phase Electrolytes. *J. Tribol.* **2023**, *145*, 071701. [CrossRef]
85. Zhang, Z.; He, F.; Huang, C.; Song, Z.; Yang, J.; Wang, X. Effect of Fe^{3+} and F^{-} on black micro-arc oxidation ceramic coating of magnesium alloy. *Int. J. Appl. Ceram. Technol.* **2022**, *19*, 2203–2212. [CrossRef]
86. Liu, C.; Zhang, W.; Xu, T.; Li, H.; Jiang, B.; Miao, X. Preparation and corrosion resistance of a self-sealing hydroxyapatite-MgO coating on magnesium alloy by microarc oxidation. *Ceram. Int.* **2022**, *48*, 13676–13683. [CrossRef]
87. Pourshadloo, M.; Jameel, M.F.; Romero-Parra, R.M.; Yeslam, H.E.; Shafik, S.S.; Kareem, A.K.; Zabibah, R.S.; Sharifianjazi, F.; Bathaei, M.S. Synthesis of TiO_2/rGO composite coatings on titanium alloys with enhanced anticorrosion performance in palmitic acid-incorporated physiological solutions. *Ceram. Int.* **2023**, *49*, 33598–33606. [CrossRef]
88. Wang, Z.X.; Zhang, J.W.; Lv, W.G.; Chen, L.Y.; Qi, F.; Chen, W.W.; Lu, S. Growth Mechanism of Ceramic Coating on ZK60 Magnesium Alloy Based on Two-Step Current-Decreasing Mode of Micro-Arc Oxidation. *Adv. Eng. Mater.* **2022**, *24*, 2101232. [CrossRef]
89. Leng, Z.; Li, T.; Wang, X.; Zhang, S.; Zhou, J. Effect of graphite content on the conductivity, wear behavior, and corrosion resistance of the organic layer on magnesium alloy MAO coatings. *Coatings* **2022**, *12*, 434. [CrossRef]
90. Cai, L.; Song, X.; Liu, C.B.; Cui, L.Y.; Li, S.Q.; Zhang, F.; Kannan, M.B.; Chen, D.C.; Zeng, R.C. Corrosion resistance and mechanisms of $Nd(NO_3)_3$ and polyvinyl alcohol organic-inorganic hybrid material incorporated MAO coatings on AZ31 Mg alloy. *J. Colloid Interface Sci.* **2023**, *630*, 833–845. [CrossRef]
91. Stojadinović, S.; Radić, N.; Vasilić, R. ZnO Particles modified MgAl Coatings with improved photocatalytic activity formed by plasma electrolytic oxidation of AZ31 magnesium alloy in aluminate electrolyte. *Catalysts* **2022**, *12*, 1503. [CrossRef]
92. Han, J.; Yu, Y.; Yang, J.; Xiaopeng, L.; Blawert, C.; Zheludkevich, M.L. Corrosion and wear performance of La_2O_3 doped plasma electrolytic oxidation coating on pure Mg. *Surf. Coat. Technol.* **2022**, *433*, 128112. [CrossRef]
93. Bordbar-Khiabani, A.; Yarmand, B.; Mozafari, M. Enhanced corrosion resistance and in-vitro biodegradation of plasma electrolytic oxidation coatings prepared on AZ91 Mg alloy using ZnO nanoparticles-incorporated electrolyte. *Surf. Coat. Technol.* **2019**, *360*, 153–171. [CrossRef]
94. Mohammed, N.B.; Daily, Z.A.; Alsharbaty, M.H.; Abullais, S.S.; Arora, S.; Lafta, H.A.; Jalil, A.T.; Almulla, A.F.; Ramírez-Coronel, A.A.; Aravindhan, S.; et al. Effect of PMMA sealing treatment on the corrosion behavior of plasma electrolytic oxidized titanium dental implants in fluoride-containing saliva solution. *Mater. Res. Express* **2022**, *9*, 125401. [CrossRef]
95. Lu, X.; Blawert, C.; Luthringer, B.J.; Zheludkevich, M.L. Controllable Degradable Plasma Electrolytic Oxidation Coated Mg Alloy for Biomedical Application. *Front. Chem. Eng.* **2022**, *4*, 748549. [CrossRef]
96. Ebrahimi, S.; Bordbar-Khiabani, A.; Yarmand, B. Immobilization of rGO/ZnO hybrid composites on the Zn substrate for enhanced photocatalytic activity and corrosion stability. *J. Alloys Compd.* **2020**, *10*, 156219. [CrossRef]

97. Patrascu, I.; Ducu, M.C.; Negrea, A.D.; Moga, S.G.; Plaiasu, A.G. Overview on plasma electrolytic oxidation of magnesium alloys for medical and engineering applications. In *IOP Conference Series: Materials Science and Engineering*; IOP Publishing: Bristol, UK, 2022; Volume 1251, p. 012001.
98. Lv, Y.; Zhang, C.; Zhang, Y.; Wang, Q.; Zhang, X.; Dong, Z. Microstructure and corrosion resistance of plasma electrolytic oxidized recycled Mg alloy. *Acta Metall. Sin. (Engl. Lett.)* **2022**, *35*, 961–974. [CrossRef]
99. Xu, L.; Zhang, D.; Su, H.; Yu, P.; Wan, Y.; Sun, H. Improving the tribocorrosion performance of plasma electrolytic oxidized coatings on AZ31B magnesium alloy using pullulan as an electrolyte additive. *Surf. Coat. Technol.* **2022**, *446*, 128754. [CrossRef]
100. Krishtal, M.M.; Katsman, A.V.; Polunin, A.V. Effects of silica nanoparticles addition on formation of oxide layers on AlSi alloy by plasma electrolytic oxidation: The origin of stishovite under ambient conditions. *Surf. Coat. Technol.* **2022**, *441*, 128556. [CrossRef]
101. Liu, X.; Liu, L.; Dong, S.; Chen, X.B.; Dong, J. Towards dense corrosion-resistant plasma electrolytic oxidation coating on Mg-Gd-Y-Zr alloy by using ultra-high frequency pulse current. *Surf. Coat. Technol.* **2022**, *447*, 128881. [CrossRef]
102. Rahmati, M.; Raeissi, K.; Toroghinejad, M.R.; Hakimizad, A.; Santamaria, M. Corrosion and wear resistance of coatings produced on AZ31 Mg alloy by plasma electrolytic oxidation in silicate-based K_2TiF_6 containing solution: Effect of waveform. *J. Magnes. Alloy.* **2022**, *10*, 2574–2587. [CrossRef]
103. Kara, R.; Zengin, H. Tribological and electrochemical corrosion properties of CNT-incorporated plasma electrolytic oxidation (PEO) coatings on AZ80 magnesium alloy. *Acta Metall. Sin. (Engl. Lett.)* **2022**, *35*, 1195–1206. [CrossRef]
104. Fattah-alhosseini, A.; Molaei, M.; Babaei, K. The effects of nano-and micro-particles on properties of plasma electrolytic oxidation (PEO) coatings applied on titanium substrates: A review. *Surf. Interfaces* **2020**, *21*, 100659. [CrossRef]
105. Lv, J.; Cheng, Y. Amorphous coatings on tantalum formed by plasma electrolytic oxidation in aluminate electrolyte and high temperature crystallization treatment. *Surf. Coat. Technol.* **2022**, *434*, 128171. [CrossRef]
106. Pezzato, L.; Lorenzetti, L.; Tonelli, L.; Bragaggia, G.; Dabalà, M.; Martini, C.; Brunelli, K. Effect of SiC and borosilicate glass particles on the corrosion and tribological behavior of AZ91D magnesium alloy after PEO process. *Surf. Coat. Technol.* **2021**, *428*, 127901. [CrossRef]
107. Bordbar-Khiabani, A.; Yarmand, B.; Sharifi-Asl, S.; Mozafari, M. Improved corrosion performance of biodegradable magnesium in simulated inflammatory condition via drug-loaded plasma electrolytic oxidation coatings. *Mater. Chem. Phys.* **2020**, *239*, 122003. [CrossRef]
108. Pezzato, L.; Gennari, C.; Franceschi, M.; Brunelli, K. Influence of silicon morphology on direct current plasma electrolytic oxidation process in AlSi10Mg alloy produced with laser powder bed fusion. *Sci. Rep.* **2022**, *12*, 14329. [CrossRef] [PubMed]
109. Santos, P.B.; de Castro, V.V.; Baldin, E.K.; Aguzzoli, C.; Longhitano, G.A.; Jardini, A.L.; Lopes, É.S.; de Andrade, A.M.; de Fraga Malfatti, C. Wear Resistance of Plasma Electrolytic Oxidation Coatings on Ti-6Al-4V Eli Alloy Processed by Additive Manufacturing. *Metals* **2022**, *12*, 1070. [CrossRef]
110. Pezzato, L.; Colusso, E.; Cerchier, P.; Settimi, A.G.; Brunelli, K. Production and Characterization of Photocatalytic PEO Coatings Containing TiO_2 Powders Recovered from Wastes. *Coatings* **2023**, *13*, 411. [CrossRef]
111. Lee, K.M.; Shin, K.R.; Namgung, S.; Yoo, B.; Shin, D.H. Electrochemical response of ZrO_2-incorporated oxide layer on AZ91 Mg alloy processed by plasma electrolytic oxidation. *Surf. Coat. Technol.* **2011**, *205*, 3779–3784. [CrossRef]
112. Sedelnikova, M.B.; Ivanov, K.V.; Ugodchikova, A.V.; Kashin, A.D.; Uvarkin, P.V.; Sharkeev, Y.; Tolkacheva, T.V.; Tolmachev, A.I.; Schmidt, J.; Egorkin, V.S.; et al. The effect of pulsed electron irradiation on the structure, phase composition, adhesion and corrosion properties of calcium phosphate coating on Mg0.8Ca alloy. *Mater. Chem. Phys.* **2023**, *294*, 126996. [CrossRef]
113. Wang, S.; Wang, Y.; Chen, J.; Zou, Y.; Ouyang, J.; Jia, D.; Zhou, Y. Simple and scalable synthesis of super-repellent multilayer nanocomposite coating on Mg alloy with mechanochemical robustness, high-temperature endurance and electric protection. *J. Magnes. Alloy.* **2022**, *10*, 2446–2459. [CrossRef]
114. Singh, A.K.; Drunka, R.; Smits, K.; Vanags, M.; Iesalnieks, M.; Joksa, A.A.; Blumbergs, I.; Steins, I. Nanomechanical and Electrochemical Corrosion Testing of Nanocomposite Coating Obtained on AZ31 via Plasma Electrolytic Oxidation Containing TiN and SiC Nanoparticles. *Crystals* **2023**, *13*, 508. [CrossRef]
115. Xue, K.; Tan, P.H.; Zhao, Z.H.; Cui, L.Y.; Kannan, M.B.; Li, S.Q.; Liu, C.B.; Zou, Y.H.; Zhang, F.; Chen, Z.Y.; et al. In vitro degradation and multi-antibacterial mechanisms of β-cyclodextrin@ curcumin embodied Mg $(OH)_2$/MAO coating on AZ31 magnesium alloy. *J. Mater. Sci. Technol.* **2023**, *132*, 179–192. [CrossRef]
116. Mohedano, M.; Blawert, C.; Zheludkevich, M.L. Silicate-based plasma electrolytic oxidation (PEO) coatings with incorporated CeO_2 particles on AM50 magnesium alloy. *Mater. Des.* **2015**, *86*, 735–744. [CrossRef]
117. Kadhum, W.R.; See, G.L.; Alhijjaj, M.; Kadhim, M.M.; Arce, F.J.; Al-Janabi, A.S.; Al-Rashidi, R.R.; Khadom, A.A. Evaluation of the Skin Permeation-Enhancing Abilities of Newly Developed Water-Soluble Self-Assembled Liquid Crystal Formulations Based on Hexosomes. *Crystals* **2022**, *12*, 1238. [CrossRef]
118. Seyyedi, M.; Molajou, A. Nanohydroxyapatite loaded-acrylated polyurethane nanofibrous scaffolds for controlled release of paclitaxel anticancer drug. *J. Res. Sci. Eng. Technol.* **2021**, *9*, 50–61.
119. Askaria, S.; Yazdani, E.; Arabuli, L.; Goldadi, H.; Marnani, S.A.S.; Emami, M. In-vitro and in-vivo examination for bioceramics degradation. *J. Compos. Compd.* **2022**, *4*, 169–177.
120. Ghasali, E.; Bordbar-Khiabani, A.; Alizadeh, M.; Mozafari, M.; Niazmand, M.; Kazemzadeh, H.; Ebadzadeh, T. Corrosion behavior and in-vitro bioactivity of porous Mg/Al_2O_3 and Mg/Si_3N_4 metal matrix composites fabricated using microwave sintering process. *Mater. Chem. Phys.* **2019**, *225*, 331–339. [CrossRef]

121. Loginova, N.; Gvozdev, M.; Osipovich, N.; Khodosovskaya, A.; Koval'chuk-Rabchinskaya, T.; Ksendzova, G.; Kotsikau, D.; Evtushenkov, A. Silver (I) complexes with phenolic Schiff bases: Synthesis, anti-bacterial evaluation and interaction with biomolecules. *ADMET DMPK* **2022**, *10*, 197–212. [CrossRef]
122. Cerchier, P.; Pezzato, L.; Brunelli, K.; Dolcet, P.; Bartolozzi, A.; Bertani, R.; Dabalà, M. Antibacterial effect of PEO coating with silver on AA7075. *Mater. Sci. Eng. C* **2017**, *75*, 554–564. [CrossRef]
123. Bordbar-Khiabani, A.; Yarmand, B.; Mozafari, M. Functional PEO layers on magnesium alloys: Innovative polymer-free drug-eluting stents. *Surf. Innov.* **2018**, *6*, 237–243. [CrossRef]
124. Kandeel, M.; Al-Taher, A. Bioinformatics of thymidine metabolism in *Trypanosoma evansi*: Exploring nucleoside deoxyribosyltransferase (NDRT) as a drug target. *Res. Sq.* **2021**. [CrossRef]
125. Polonchuk, L.; Gentile, C. Current state and future of 3D bioprinted models for cardio-vascular research and drug development. *ADMET DMPK* **2021**, *9*, 231–242. [CrossRef] [PubMed]
126. Ghanbari, A.; Bordbar-Khiabani, A.; Warchomicka, F.; Sommitsch, C.; Yarmand, B.; Zamanian, A. PEO/Polymer hybrid coatings on magnesium alloy to improve biodegradation and biocompatibility properties. *Surf. Interfaces* **2023**, *36*, 102495. [CrossRef]
127. Alquhaidan, M.; Kandeel, M. Gene expression of multidrug-resistant ATP-binding cassette transporter (MDR1/ABCB1) in bovine mastitis. *Trop. J. Pharm. Res.* **2018**, *17*, 2335–2340. [CrossRef]
128. Kadhum, W.R.; Al-Zuhairy, S.A.; Mohamed, M.B.; Abdulrahman, A.Y.; Kadhim, M.M.; Alsadoon, Z.; Teoh, T.C. A Nanotechnological Approach for Enhancing the Topical Drug Delivery by Newly Developed Liquid Crystal Formulations. *Int. J. Drug Deliv. Technol.* **2021**, *11*, 716–720. [CrossRef]
129. Al-Zuhairy, S.A.; Kadhum, W.R.; Alhijjaj, M.; Kadhim, M.M.; Al-Janabi, A.S.; Salman, A.W.; Al-Sharifi, H.K.; Khadom, A.A. Development and Evaluation of Biocompatible Topical Petrolatum-liquid Crystal Formulations with Enhanced Skin Permeation Properties. *J. Oleo Sci.* **2022**, *71*, 459–468. [CrossRef] [PubMed]
130. Gani, I.H.; Al-Obaidi, Z. Molecular docking studies of tyrosine kinase inhibitors: Exemplified protocol to advance pharmaceutical education in medicinal chemistry. *Pharm. Educ.* **2022**, *22*, 110–114. [CrossRef]
131. Liu, R.; Xu, D.; Liu, Y.; Wu, L.; Yong, Q.; Xie, Z.H. Enhanced corrosion protection for MAO coating on magnesium alloy by the synergism of LDH doping with deposition of 8HQ inhibitor film. *Ceram. Int.* **2023**, *49*, 30039–30048. [CrossRef]
132. Khiabani, A.B.; Rahimi, S.; Yarmand, B.; Mozafari, M. Electrophoretic deposition of graphene oxide on plasma electrolytic oxidized-magnesium implants for bone tissue engineering applications. *Mater. Today Proc.* **2018**, *5*, 15603–15612. [CrossRef]
133. Johari, N.A.; Alias, J.; Zanurin, A.; Mohamed, N.S.; Alang, N.A.; Zain, M.Z. Anti-corrosive coatings of magnesium: A review. *Mater. Today Proc.* **2022**, *48*, 1842–1848. [CrossRef]
134. Zhang, Y.; Li, N.; Ling, N.; Zhang, J.; Wang, L. Enhanced long-term corrosion resistance of Mg alloys by superhydrophobic and self-healing composite coating. *Chem. Eng. J.* **2022**, *449*, 137778. [CrossRef]
135. Li, B.; Wang, L.; Su, Y.; Qiu, R.; Zhang, Z.; Ouyang, Y. Refreshable self-polishing superhydrophobic coating on Mg alloy to prohibit corrosion and biofouling in marine environment. *Colloids Surf. A Physicochem. Eng. Asp.* **2022**, *651*, 129693. [CrossRef]
136. Telmenbayar, L.; Ramu, A.G.; Erdenebat, T.O.; Choi, D. Anticorrosive lanthanum embedded PEO/GPTMS coating on magnesium alloy by plasma electrolytic oxidation with silanization. *Mater. Today Commun.* **2022**, *33*, 104662. [CrossRef]
137. Wang, Y.; You, Z.; Ma, K.; Dai, C.; Wang, D.; Wang, J. Corrosion resistance of a superhydrophobic calcium carbonate coating on magnesium alloy by ultrasonic cavitation-assisted chemical conversion. *Corros. Sci.* **2023**, *211*, 110841. [CrossRef]
138. Wang, H.; Song, Y.; Chen, X.; Tong, G.; Zhang, L. Microstructure and corrosion behavior of PEO-LDHs-SDS superhydrophobic composite film on magnesium alloy. *Corros. Sci.* **2022**, *208*, 110699. [CrossRef]
139. Song, J.; Gao, Y.; Liu, C.; Chen, Z. The effect of Sr addition on the microstructure and corrosion behaviour of a Mg-Zn-Ca alloy. *Surf. Coat. Technol.* **2022**, *437*, 128328. [CrossRef]
140. Li, J.; Zhang, Z.; Guo, Z.; Yang, Z.; Qian, W.; Chen, Y.; Li, H.; Zhao, Q.; Xing, Y.; Zhao, Y. Improved corrosion resistance of ZrO_2/MgO coating for magnesium alloys by manipulating the pore structure. *J. Mater. Res. Technol.* **2023**, *24*, 2403–2415. [CrossRef]
141. Rehman, Z.U.; Uzair, M.; Lim, H.T.; Koo, B.H. Structural and electrochemical properties of the catalytic CeO_2 nanoparticles-based PEO ceramic coatings on AZ91 Mg alloy. *J. Alloys Compd.* **2017**, *726*, 284–294. [CrossRef]
142. Lim, T.S.; Ryu, H.S.; Hong, S.H. Electrochemical corrosion properties of CeO_2-containing coatings on AZ31 magnesium alloys prepared by plasma electrolytic oxidation. *Corros. Sci.* **2012**, *62*, 104–111. [CrossRef]
143. Lou, B.S.; Lee, J.W.; Tseng, C.M.; Lin, Y.Y.; Yen, C.A. Mechanical property and corrosion resistance evaluation of AZ31 magnesium alloys by plasma electrolytic oxidation treatment: Effect of MoS_2 particle addition. *Surf. Coat. Technol.* **2018**, *350*, 813–822. [CrossRef]
144. Vatan, H.N.; Ebrahimi-Kahrizsangi, R.; Kasiri-Asgarani, M. Structural, tribological and electrochemical behavior of SiC nanocomposite oxide coatings fabricated by plasma electrolytic oxidation (PEO) on AZ31 magnesium alloy. *J. Alloys Compd.* **2016**, *683*, 241–255. [CrossRef]
145. Vatan, H.N.; Ebrahimi-Kahrizsangi, R.; Asgarani, M.K. Effect of WC nano-powder on properties of plasma electrolytic oxidation coating fabricated on AZ31B alloy. *Int. J. Electrochem. Sci.* **2016**, *11*, 929–943. [CrossRef]
146. Zhao, J.; Xie, X.; Zhang, C. Effect of the graphene oxide additive on the corrosion resistance of the plasma electrolytic oxidation coating of the AZ31 magnesium alloy. *Corros. Sci.* **2017**, *114*, 146–155. [CrossRef]

147. Seyfoori, A.; Mirdamadi, S.; Seyedraoufi, Z.S.; Khavandi, A.; Aliofkhazraei, M. Synthesis of biphasic calcium phosphate containing nanostructured films by micro arc oxidation on magnesium alloy. *Mater. Chem. Phys.* **2013**, *142*, 87–94. [CrossRef]
148. Mashtalyar, D.V.; Gnedenkov, S.V.; Sinebryukhov, S.L.; Imshinetskiy, I.M. Plasma electrolytic oxidation of the magnesium alloy MA8 in electrolytes containing TiN nanoparticles. *J. Mater. Sci. Technol.* **2017**, *33*, 461–468. [CrossRef]
149. Lu, X.; Blawert, C.; Huang, Y.; Ovri, H.; Zheludkevich, M.L.; Kainer, K.U. Plasma electrolytic oxidation coatings on Mg alloy with addition of SiO_2 particles. *Electrochim. Acta* **2016**, *187*, 20–33. [CrossRef]
150. Lu, X.; Sah, S.P.; Scharnagl, N.; Störmer, M.; Starykevich, M.; Mohedano, M.; Blawert, C.; Zheludkevich, M.L.; Kainer, K.U. Degradation behavior of PEO coating on AM50 magnesium alloy produced from electrolytes with clay particle addition. *Surf. Coat. Technol.* **2015**, *269*, 155–169. [CrossRef]
151. Chen, F.; Zhang, Y.; Zhang, Y. Effect of graphene on micro-structure and properties of MAO coating prepared on Mg-Li alloy. *Int. J. Electrochem. Sci.* **2017**, *12*, 6081–6091. [CrossRef]
152. Wen, C.; Zhan, X.; Huang, X.; Xu, F.; Luo, L.; Xia, C. Characterization and corrosion properties of hydroxyapatite/graphene oxide bio-composite coating on magnesium alloy by one-step micro-arc oxidation method. *Surf. Coat. Technol.* **2017**, *317*, 125–133. [CrossRef]
153. Xiong, Y.; Hu, X.; Song, R. Characteristics of CeO_2/ZrO_2-HA composite coating on ZK60 magnesium alloy. *J. Mater. Res.* **2017**, *32*, 1073–1082. [CrossRef]
154. Keyvani, A.; Zamani, M.; Bahamirian, M.; Nikoomanzari, E.; Fattah-Alhosseini, A.; Sina, H. Role of incorporation of ZnO nanoparticles on corrosion behavior of ceramic coatings developed on AZ31 magnesium alloy by plasma electrolytic oxidation technique. *Surf. Interfaces* **2021**, *22*, 100728. [CrossRef]
155. Asgari, M.; Aliofkhazraei, M.; Darband, G.B.; Rouhaghdam, A.S. Evaluation of alumina nanoparticles concentration and stirring rate on wear and corrosion behavior of nanocomposite PEO coating on AZ31 magnesium alloy. *Surf. Coat. Technol.* **2017**, *309*, 124–135. [CrossRef]
156. Ma, C.; Lu, Y.; Sun, P.; Yuan, Y.; Jing, X.; Zhang, M. Characterization of plasma electrolytic oxidation coatings formed on Mg–Li alloy in an alkaline polyphosphate electrolyte. *Surf. Coat. Technol.* **2011**, *206*, 287–294. [CrossRef]
157. Pezzato, L.; Angelini, V.; Brunelli, K.; Martini, C.; Dabalà, M. Tribological and corrosion behavior of PEO coatings with graphite nanoparticles on AZ91 and AZ80 magnesium alloys. *Trans. Nonferrous Met. Soc. China* **2018**, *28*, 259–272. [CrossRef]
158. Mortezanejad, E.; Atapour, M.; Salimijazi, H.; Alhaji, A.; Hakimizad, A. Wear and corrosion behavior of aluminate-and phosphate-based plasma electrolytic oxidation coatings with polytetrafluoroethylene nanoparticles on AZ80 Mg alloy. *J. Mater. Eng. Perform.* **2021**, *30*, 4030–4044. [CrossRef]
159. Zehra, T.; Patil, S.A.; Shrestha, N.K.; Fattah-Alhosseini, A.; Kaseem, M. Anionic assisted incorporation of WO_3 nanoparticles for enhanced electrochemical properties of AZ31 Mg alloy coated via plasma electrolytic oxidation. *J. Alloys Compd.* **2022**, *916*, 165445. [CrossRef]
160. Espiritu, J.; Sefa, S.; Ćwieka, H.; Greving, I.; Flenner, S.; Willumeit-Römer, R.; Seitz, J.M.; Zeller-Plumhoff, B. Detailing the influence of PEO-coated biodegradable Mg-based implants on the lacuno-canalicular network in sheep bone: A pilot study. *Bioact. Mater.* **2023**, *26*, 14–23. [CrossRef]
161. Bordbar-Khiabani, A.; Bahrampour, S.; Mozafari, M.; Gasik, M. Surface functionalization of anodized tantalum with Mn_3O_4 nanoparticles for effective corrosion protection in simulated inflammatory condition. *Ceram. Int.* **2022**, *48*, 3148–3156. [CrossRef]
162. Pezzato, L.; Coelho, L.B.; Bertolini, R.; Settimi, A.G.; Brunelli, K.; Olivier, M.; Dabalà, M. Corrosion and mechanical properties of plasma electrolytic oxidation-coated AZ80 magnesium alloy. *Mater. Corros.* **2019**, *70*, 2103–2112. [CrossRef]
163. Bordbar-Khiabani, A.; Yarmand, B.; Mozafari, M. Effect of ZnO pore-sealing layer on anti-corrosion and in-vitro bioactivity behavior of plasma electrolytic oxidized AZ91 magnesium alloy. *Mater. Lett.* **2020**, *258*, 126779. [CrossRef]
164. Çelik, A.; Bozkurt, Y.B. Improvement of tribological performance of AZ31 biodegradable alloy by TiN-based PVD coatings. *Tribol. Int.* **2022**, *173*, 107684. [CrossRef]
165. Niraj, N.; Pandey, K.M.; Dey, A. Tribological behaviour of Magnesium Metal Matrix Composites reinforced with fly ash cenosphere. *Mater. Today Proc.* **2018**, *5*, 20138–21044. [CrossRef]
166. Sidhu, V.P.; Marchi, J.; Borges, R.; Ahmadi, E. Surface modification of metallic orthopedic implants for anti-pathogenic characteristics. *J. Compos. Compd.* **2022**, *4*, 51–60.
167. Jagadeesh, G.V.; Gangi Setti, S. Tribological performance evaluation of ball burnished magnesium alloy for bioresorbable implant applications. *J. Mater. Eng. Perform.* **2022**, *31*, 1170–1186. [CrossRef]
168. Singh, H.; Lodhi, A.P.S.; Verma, T.; Kumar, D.; Jain, J. Tribological response of binary Mg-xZn (Where X = 1, 3 and 6 wt%) alloys. *Mater. Today Proc.* **2021**, *41*, 786–790. [CrossRef]
169. Fattah-alhosseini, A.; Molaei, M.; Nouri, M.; Babaei, K. Antibacterial activity of bioceramic coatings on Mg and its alloys created by plasma electrolytic oxidation (PEO): A review. *J. Magnes. Alloy.* **2022**, *10*, 81–96. [CrossRef]
170. Esmaeili, M.; Tadayonsaidi, M.; Ghorbanian, B. The effect of PEO parameters on the properties of biodegradable Mg alloys: A review. *Surf. Innov.* **2021**, *9*, 184–198. [CrossRef]
171. Fattah-alhosseini, A.; Molaei, M.; Attarzadeh, N.; Babaei, K.; Attarzadeh, F. On the enhanced antibacterial activity of plasma electrolytic oxidation (PEO) coatings that incorporate particles: A review. *Ceram. Int.* **2020**, *46*, 20587–20607. [CrossRef]
172. Chaharmahali, R.; Fattah-Alhosseini, A.; Esfahani, H. Increasing the in-vitro corrosion resistance of AZ31B-Mg alloy via coating with hydroxyapatite using plasma electrolytic oxidation. *J. Asian Ceram. Soc.* **2020**, *8*, 39–49. [CrossRef]

173. Fattah-alhosseini, A.; Chaharmahali, R.; Alizad, S.; Kaseem, M. Corrosion behavior of composite coatings containing hydroxyapatite particles on Mg alloys by plasma electrolytic oxidation: A review. *J. Magnes. Alloy.* **2023**, *11*, 2999–3011. [CrossRef]
174. Molaei, M.; Babaei, K.; Fattah-alhosseini, A. Improving the wear resistance of plasma electrolytic oxidation (PEO) coatings applied on Mg and its alloys under the addition of nano-and micro-sized additives into the electrolytes: A review. *J. Magnes. Alloy.* **2021**, *9*, 1164–1186. [CrossRef]
175. Buling, A.; Zerrer, J. Increasing the application fields of magnesium by ultraceramic®: Corrosion and wear protection by plasma electrolytical oxidation (PEO) of Mg alloys. *Surf. Coat. Technol.* **2019**, *369*, 142–155. [CrossRef]
176. Asgari, M.; Aliofkhazraei, M.; Darband, G.B.; Rouhaghdam, A.S. How nanoparticles and submicron particles adsorb inside coating during plasma electrolytic oxidation of magnesium? *Surf. Coat. Technol.* **2020**, *383*, 125252. [CrossRef]
177. Long, Y.; Wu, L.; Zhang, Z.; Atrens, A.; Pan, F.; Tang, A.; Zhang, G. Enhanced corrosion resistance of anodic films containing alumina nanoparticles on as-rolled AZ31 alloy. *Int. J. Electrochem. Sci.* **2018**, *13*, 7157–7174. [CrossRef]
178. Gheytani, M.; Bagheri, H.R.; Masiha, H.R.; Aliofkhazraei, M.; Sabour Rouhaghdam, A.; Shahrabi, T. Effect of SMAT preprocessing on MAO fabricated nanocomposite coating. *Surf. Eng.* **2014**, *30*, 244–255. [CrossRef]
179. Gnedenkov, S.V.; Sinebryukhov, S.L.; Mashtalyar, D.V.; Imshinetskiy, I.M.; Samokhin, A.V.; Tsvetkov, Y.V. Fabrication of coatings on the surface of magnesium alloy by plasma electrolytic oxidation using ZrO_2 and SiO_2 nanoparticles. *J. Nanomater.* **2015**, *2015*, 154298. [CrossRef]
180. Tezcan, M.M.; Yetgin, A.G.; Canakoglu, A.I.; Cevher, B.; Turan, M.; Ayaz, M.; Vasko, M.; Handrik, M.; Jakubovicova, L.; Kopas, P.; et al. Investigation of the effects of the equivalent circuit parameters on induction motor torque using three different equivalent circuit models. *MATEC Web Conf.* **2018**, *157*, 11. [CrossRef]
181. Imshinetsky, I.M.; Gnedenkov, S.V.; Sinebryukhov, S.L.; Mashtalyar, D.V.; Samokhin, A.V.; Tsvetkov, Y.V. Incorporation of Composite Zirconia-Silica Nanoparticles into PEO-Coatings on Magnesium Alloys. *Defect Diffus. Forum* **2018**, *386*, 321–325. [CrossRef]
182. Atapour, M.; Blawert, C.; Zheludkevich, M.L. The wear characteristics of CeO_2 containing nanocomposite coating made by aluminate-based PEO on AM 50 magnesium alloy. *Surf. Coat. Technol.* **2019**, *357*, 626–637. [CrossRef]
183. Madhankumar, A.; Thangavel, E.; Ramakrishna, S.; Obot, I.B.; Jung, H.C.; Shin, K.S.; Gasem, Z.M.; Kim, H.; Kim, D.E. Multifunctional ceramic hybrid coatings on biodegradable AZ31 Mg implants: Electrochemical, tribological and quantum chemical aspects for orthopaedic applications. *Rsc Adv.* **2014**, *4*, 24272–24285. [CrossRef]
184. Yu, L.; Cao, J.; Cheng, Y. An improvement of the wear and corrosion resistances of AZ31 magnesium alloy by plasma electrolytic oxidation in a silicate–hexametaphosphate electrolyte with the suspension of SiC nanoparticles. *Surf. Coat. Technol.* **2015**, *276*, 266–278. [CrossRef]
185. Vatan, H.N.; Kahrizsangi, R.E.; Asgarani, M.K. Growth, corrosion and wear resistance of SiC nanoparticles embedded MAO coatings on AZ31B magnesium alloy. *Prot. Met. Phys. Chem. Surf.* **2016**, *52*, 859–868. [CrossRef]
186. Ebrahimi-Kahrizsangi, R.; Vatan, H.V. Improvement of Wear Resistance of AZ31 B Mg Alloy by Applying Oxide-Sic Nanocomposite Coating via Plasma Electrolytic Oxidation. In Proceedings of the 2nd World Congress on New Technologies 2016, Budapest, Hungary, 18–19 August 2016. [CrossRef]
187. Wang, S.Y.; Si, N.C.; Xia, Y.P.; Liu, L. Influence of nano-SiC on microstructure and property of MAO coating formed on AZ91D magnesium alloy. *Trans. Nonferrous Met. Soc. China* **2015**, *25*, 1926–1934. [CrossRef]
188. Vatan, H.N.; Ebrahimi-Kahrizsangi, R.; Kasiri-Asgaranim, M. Wear and Corrosion Performance of PEO-synthesized SiC Nanocomposite Coatings: Effect of Processing Time and Current Density. *Int. J. Electrochem. Sci.* **2016**, *11*, 5631–5654. [CrossRef]
189. NasiriVatan, H.; Ebrahimi-Kahrizsangi, R.; Asgarani, M.K. Tribological performance of PEO-WC nanocomposite coating on Mg alloys deposited by plasma electrolytic oxidation. *Tribol. Int.* **2016**, *98*, 253–260. [CrossRef]
190. Nasiri Vatan, H.; Adabi, M. Investigation of wear and corrosion resistance of nanocomposite coating formed on AZ31B Mg alloy by plasma electrolytic oxidation. *Trans. Inst. Met. Finish.* **2017**, *95*, 308–315. [CrossRef]
191. Polunin, A.V.; Borgardt, E.D.; Shafeev, M.R.; Krishtal, M.M. The effect of tungsten carbide nanoparticles added to electrolyte on the composition and properties of oxide layers formed by plasma electrolytic oxidation on pre-eutectic silumin. *J. Phys. Conf. Ser.* **2019**, *1396*, 012032. [CrossRef]
192. Imshinetsky, I.M.; Mashtalyar, D.V.; Sunebryukhov, S.L.; Gnedenkov, S.V. Mechanical properties of PEO-coatings on the surface of magnesium alloy MA8 modified by TiN nanoparticles. *AIP Conf. Proc.* **2017**, *1874*, 040012. [CrossRef]
193. Mashtalyar, D.V.; Sinebryukhov, S.L.; Imshinetskiy, I.M.; Gnedenkov, A.S.; Nadaraia, K.V.; Ustinov, A.Y.; Gnedenkov, S.V. Hard wearproof PEO-coatings formed on Mg alloy using TiN nanoparticles. *Appl. Surf. Sci.* **2020**, *503*, 144062. [CrossRef]
194. Li, Z.; Wang, X.; Dong, X.; Hu, F.; Liu, S.; Zhang, M.; Yuan, T.; Yu, Y.; Kuang, Q.; Ren, Q.; et al. Creating high-performance bifunctional composite coatings on magnesium−8lithium alloy through electrochemical surface engineering with highly enhanced corrosion and wear protection. *J. Alloys Compd.* **2020**, *818*, 153341. [CrossRef]
195. Fu, J.-G.; Ma, S.-L.; Zhu, X.-H.; Xu, C.-Q.; Yan, Z.-J.; Cheng, D.; Ma, C.-S. Influence of solid lubricant WS_2 on the tribological properties of plasma electrolytic oxidation coating of ZL109. *Mater. Res. Expr.* **2020**, *6*, 1265c8.
196. Nasiri Vatan, H.; Adabi, M. Investigation of tribological behavior of ceramic–graphene composite coating produced by plasma electrolytic oxidation. *Trans. Indian Inst. Met.* **2018**, *71*, 1643–1652. [CrossRef]
197. Zhang, Y.; Chen, F.; Zhang, Y.; Du, C. [1]Influence of graphene oxide additive on the tribological and electrochemical corrosion properties of a PEO coating prepared on AZ31 magnesium alloy. *Tribol. Int.* **2020**, *146*, 106135. [CrossRef]

198. Mozafarnia, H.; Fattah-Alhosseini, A.; Chaharmahali, R.; Nouri, M.; Keshavarz, M.K.; Kaseem, M. Corrosion, wear, and antibacterial behaviors of hydroxyapatite/MgO composite PEO coatings on AZ31 Mg alloy by incorporation of TiO_2 nanoparticles. *Coatings* **2022**, *12*, 1967. [CrossRef]
199. Zheng, Z.; Zhao, M.C.; Tan, L.; Zhao, Y.C.; Xie, B.; Yin, D.; Yang, K.; Atrens, A. Corrosion behavior of a self-sealing coating containing CeO_2 particles on pure Mg produced by micro-arc oxidation. *Surf. Coat. Technol.* **2020**, *386*, 125456. [CrossRef]
200. da Silva Rodrigues, J.; Antonini, L.M.; da Cunha Bastos, A.A.; Zhou, J.; de Fraga Malfatti, C. Corrosion resistance and tribological behavior of ZK30 magnesium alloy coated by plasma electrolytic oxidation. *Surf. Coat. Technol.* **2021**, *410*, 126983. [CrossRef]
201. Babaei, K.; Fattah-Alhosseini, A.; Molaei, M. The effects of carbon-based additives on corrosion and wear properties of Plasma electrolytic oxidation (PEO) coatings applied on Aluminum and its alloys: A review. *Surf. Interfaces* **2020**, *21*, 100677. [CrossRef]
202. Polunin, A.V.; Cheretaeva, A.O.; Borgardt, E.D.; Rastegaev, I.A.; Krishtal, M.M.; Katsman, A.V.; Yasnikov, I.S. Improvement of oxide layers formed by plasma electrolytic oxidation on cast AlSi alloy by incorporating TiC nanoparticles. *Surf. Coat. Technol.* **2021**, *423*, 127603. [CrossRef]
203. Meenashisundaram, G.K.; Gupta, M. Synthesis and characterization of high performance low volume fraction TiC reinforced Mg nanocomposites targeting biocompatible/structural applications. *Mater. Sci. Eng.* **2015**, *627*, 306–315. [CrossRef]
204. Jonda, E.; Łatka, L.; Godzierz, M.; Maciej, A. Investigations of microstructure and corrosion resistance of WC-Co and WC-Cr_3C_2-Ni coatings deposited by HVOF on magnesium alloy substrates. *Surf. Coat. Technol.* **2023**, *459*, 129355. [CrossRef]
205. Lou, B.S.; Lin, Y.Y.; Tseng, C.M.; Lu, Y.C.; Duh, J.G.; Lee, J.W. Plasma electrolytic oxidation coatings on AZ31 magnesium alloys with Si_3N_4 nanoparticle additives. *Surf. Coat. Technol.* **2017**, *332*, 358–367. [CrossRef]
206. Tonelli, L.; Pezzato, L.; Dolcet, P.; Dabalà, M.; Martini, C. Effects of graphite nano-particle additions on dry sliding behaviour of plasma-electrolytic-oxidation-treated EV31A magnesium alloy against steel in air. *Wear* **2018**, *404*, 122–132. [CrossRef]
207. Aydin, F.; Ayday, A.; Turan, M.E.; Zengin, H. Role of graphene additive on wear and electrochemical corrosion behaviour of plasma electrolytic oxidation (PEO) coatings on Mg–MWCNT nanocomposite. *Surf. Eng.* **2020**, *36*, 791–799. [CrossRef]
208. Safari, N.; Golafshan, N.; Kharaziha, M.; Reza Toroghinejad, M.; Utomo, L.; Malda, J.; Castilho, M. Stable and antibacterial magnesium–graphene nanocomposite-based implants for bone repair. *ACS Biomater. Sci. Eng.* **2020**, *6*, 6253–6262. [CrossRef]
209. Zhang, Y.; Chen, F.; Zhang, Y.; Liu, Z.; Wang, X.; Du, C. Influence of graphene oxide on the antiwear and antifriction performance of MAO coating fabricated on MgLi alloy. *Surf. Coat. Technol.* **2019**, *364*, 144–156. [CrossRef]